SERI/STR-211-3104
DE87001142

January 1987

Research on High-Efficiency, Stacked, Multi-Junction, Amorphous Silicon Alloy Thin-Film Solar Cells

Semiannual Subcontract Report 15 October 1985 - 30 April 1986

V. Dalal
Spire Corporation
Bedford, MA

Prepared under Subcontract No. ZB-4-03055-1

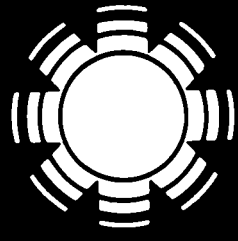

SERI

Solar Energy Research Institute
A Division of Midwest Research Institute

1617 Cole Boulevard
Golden, Colorado 80401-3393

Operated for the
U.S. Department of Energy
under Contract No. DE-AC02-83CH10093

Printed in the United States of America
Available from:
National Technical Information Service
U.S. Department of Commerce
5285 Port Royal Road
Springfield, VA 22161

Price: Microfiche A01
Printed Copy A04

Codes are used for pricing all publications. The code is determined by the number of pages in the publication. Information pertaining to the pricing codes can be found in the current issue of the following publications, which are generally available in most libraries: *Energy Research Abstracts, (ERA); Government Reports Announcements* and Index (*GRA* and I); *Scientific and Technical Abstract Reports (STAR);* and publication, NTIS-PR-360 available from NTIS at the above address.

SERI/STR-211-3104
UC Category: 63
DE87001142

SERI/STR--211-3104

DE87 001142

Research on High-Efficiency, Stacked, Multi-Junction, Amorphous Silicon Alloy Thin-Film Solar Cells

Semiannual Subcontract Report
15 October 1985 - 30 April 1986

V. Dalal
Spire Corporation
Bedford, MA

January 1987

SERI Technical Monitor:
W. Luft

Prepared under Subcontract No. ZB-4-03055-1

Solar Energy Research Institute
A Division of Midwest Research Institute

1617 Cole Boulevard
Golden, Colorado 80401-3393

Prepared for the
U.S. Department of Energy
Contract No. DE-AC02-83CH10093

ACKNOWLEDGEMENTS

The following personnel participated in the research reported in this report:

Spire Corporation:	Julio Bragagnolo, Program Manager
	Vikram Dalal, Principal Investigator
	Anton Greenwald
	Ashok Vaseashta
	James Booker
	Mark Leonard
	Stephen Tobin
Polaroid:	Camille Fuleihan
	Charles Botts
	Floyd Berry
University of Delaware:	Bill Baron
	Steven Hegedus
	Kenneth Schubert
Drexel University:	Allen Rothwarf (consultant)

TABLE OF CONTENTS

LIST OF ILLUSTRATIONS

LIST OF TABLES

SECTION 1

SUMMARY

1.1 OBJECTIVE

The objective of the research performed under this contract is to develop high efficiency multi-junction amorphous silicon alloy solar cells. Specifically, it aims to investigate the deposition of a-Si:H and a-(Si,Ge):H alloys, to perform chemical, structural, optical and electronic characterization of those materials and to fabricate and analyze a-Si:H/a-(Si,Ge):H high-efficiency tandem solar cells.

1.2 DISCUSSION

The approach used to achieve the program objectives is to pursue four technical tasks, dealing with the preparation and characterization of semiconducting and non-semiconducting materials and single- and multi-junction devices. The status of the research at the beginning of the period reported here can be briefly sumarized by listing the key achievements of the first two years (see V. Dalal et al., Annual Report to SERI for Phase II of Subcontract ZB-04-03055 (February 1986)):

a) Semiconductor Materials Research

- Construction of single-chamber and a plasma-isolated multi-chamber reactors.
- Optimization of growth conditions in both reactors to yield high-quality material with high light-to-dark conductivity ratios ($>10^6$).

b) Non-Semiconductor Materials Research

- Construction of a reactor for the chemical vapor deposition of textured SnO_2:F for enhanced photon absorption.

c) Single-Junction Cell Research

- Development of an 8.6% efficient a-Si:H p-i-n solar cell.
- Development of a 6.8% efficient a-(Si,Ge):H p-i-n solar cell.

d) Tandem-Junction Cell Research

- Development of a 6.7% efficient a-Si:H/a-(Si,Ge):H solar cell.
- Development of new technique for measurement of quantum efficiency of tandem cells.

This report describes the work performed during the first half of the third year of this three year project. A discussion of the progress made during this period follows.

1.2.1 Semiconductor Materials Research

A new plasma isolated, two chamber, hot wall glow discharge reactor (R3) was put into operation. Good quality, p+, i and n+ a-Si:H layers were grown in this reactor, with i-layers having photo-to-dark conductivity ratios near 10^6 and $E_g = 1.78\text{-}1.80$ eV. For the growth of high quality devices in R3, layer thickness uniformity needs to be improved. Also, contamination of the i-layer presumably caused by B_2H_6 desorbed from cold areas of the reactor, results in poor device fill-factor and needs to be corrected.

1.2.2 Non-Semiconductor Materials Research

A CVD pyrolytic reactor for the deposition of SnO_2:F layers on glass was put into operation. Process conditions for the deposition of both textured and specular SnO_2:F layers with high transparency and low sheet resistance were developed. Film quality factors, defined as the ratio of absorptivity to resistivity, attained values up to 3.5 for specular layers, among the highest reported anywhere.

A process to deposit high reflectivity, two-layer back contacts of Ti/Ag was developed. The reflectance of Ti/Ag samples exceeded 95%.

1.2.3 Single-Junction Cell Research

Two samples yielding a-Si:H cells with up to 9.1% efficiency and 0.1 cm^2 area have been made in our multi-sector RF glow discharge deposition chamber. In one case, textured and specular SnO_2:F/glass superstrates, made in our CVD reactor, were used to demonstrate the effect of texture in increasing conversion efficiency, with the high efficiency cell made on the textured sample. This established for the first time our ability to deposit all the layers of a high performance device in-house.

Graded bandgap a-(Si,Ge):H cells of up to 7.5% conversion efficiency were also made in the multi-sector reactor. The Ge atomic fraction in the lower bandgap region of the graded i-layer was determined by Auger Electron Spectroscopy to be as high as 0.39, suggesting that $E_g \approx 1.5$ eV in that region.

All our high efficiency cells were fabricated with Al back contacts. However, enhanced photovoltaic performance, with Quantum Efficiency gains of over 7% for both a-Si:H and a-(Si,Ge):H cells, was demonstrated with the Ti/Ag back contact technology, although some lack of reproducibility in device fill-factor was noted.

1.2.4 Multi-Junction Cell Research

Multi-junction a-Si:H/a-(Si,Ge):H solar cells with up to 7.2% conversion efficiency were made in our multi-sector deposition chamber. A modeling effort to predict tandem cell performance was started. Based on preliminary results, tandem efficiencies in the range of 8-9% can be achieved with our present single-junction cells.

1.3 CONCLUSIONS

As follows from the experimental results obtained during this period, most of the elements necessary for the fabrication of high efficiency a-Si:H alloy solar cells have been developed. The key barrier to higher performance is the quality of the a-(Si,Ge):H i-layer in the bottom cell of the tandem in the range of $E_g \leq 1.5$ eV. In the following period, the effort will focus on improving a-(Si,Ge):H i-layer quality in the range $E_g \leq 1.5$ eV.

SECTION 2

SEMICONDUCTOR MATERIALS RESEARCH

2.1 MATERIAL GROWTH IN HOT-WALL DEPOSITION SYSTEM

A new RF glow discharge reactor for the deposition of a-Si:H alloy devices (R3) was completed during this period.* The key design features of this reactor are:

a) Two plasma-isolated, vacuum-connected deposition chambers (dopant and intrinsic).

b) Large-area triode electrode geometry.

c) Hot-wall sample temperature control.

Good quality p^+, i and n^+ a-Si:H layers were obtained in R3 (see Table 2-1). The process parameters were essentially the same as those used in our single and multi-chamber reactors. The high photo-to-dark i-layer conductivity ratios ($\approx 10^{+6}$) compare well with the best values obtained in those reactors.

TABLE 2-1. DARK AND PHOTOCONDUCTIVITY OF a-Si:H LAYERS FROM R3.

SAMPLE	TYPE	E_g (eV)	σ PHOTO $(ohm\text{-}cm)^{-1}$	σ DARK $(ohm\text{-}cm)^{-1}$	σPHOTO/σDARK
30002A	p^+	1.73	1.3×10^{-5}	1.3×10^{-5}	1.0
30003B	n^+	1.75	7.3×10^{-3}	6.8×10^{-3}	1.07
30016A	i	1.76	2.0×10^{-10}	1.9×10^{-4}	9.7×10^{5}
30023A	i	1.80	2.5×10^{-10}	2.1×10^{-4}	8.6×10^{5}

The effort to develop a-Si:H alloy devices in R3 has been delayed by two problems: dopant (B_2H_6) contamination of the i-layer and layer non-uniformity. We use device data to identify dopant contamination. Figure 2-1 shows the ratio of the reverse voltage-bias to the short-circuit quantum efficiencies QE(-1V)/QE(0V) for cell 30008-D7. The I-V parameters of this cell are: V_{OC} = 715 mW, J_{SC} = 11.6 mA/cm^3, FF = 59.5% and Eff = 4.9%

* R3 was built with Polaroid funds.

The high value of the QE ratio $\approx$ 1.18 for λ = 400 nm is consistent with a sub-optimum i-layer drift field near the p^+-i interface, a sure indicator of the presence of B in that region. This occurs even when a SiH_4 plasma is run in both chambers between the p^+ and i-layer depositions. Dopant contamination, not expected in a hot-wall reactor, is believed to arise from B_2H_6 lingering in the cold, non-isolated magnetic feedthrough used for sample transport. This design problem is presently being corrected.

2.2 LAYER UNIFORMITY IN HOT-WALL REACTOR

A major problem in using this reactor for device deposition became quickly apparent when layer uniformity was evaluated. A scanning reflectometer was used to map layer thickness over a 10 cm x 10 cm area sample. A typical pattern is shown in Figure 2-2. The thickness difference between two points (1 and 2) in the sample, separated by N fringes, is given by:

$$t(1)-t(2) = N \lambda/2n = 77.8 \times N \text{ [nm]}$$

where n = 4.07 is the refractive index of a-Si:H and λ = 633 nm is the wavelength of the reflectometer light source. Small phase shifts that depend on the attenuation coefficient of a-Si:H have been neglected. The sample thickness t(1) = 770 nm at the thickest point (marked with an * in the figure), was calculated from photon transmision vs. wavelength data. For this sample, the variation from the thickest to the thinnest point is about 50%. This is not acceptable in device fabrication.

We have chosen not to pursue device or materials deposition until the uniformity problem is solved. It is expected that uniform layers will be achieved shortly by correcting plasma inhomogeneities associated with "hot spots".

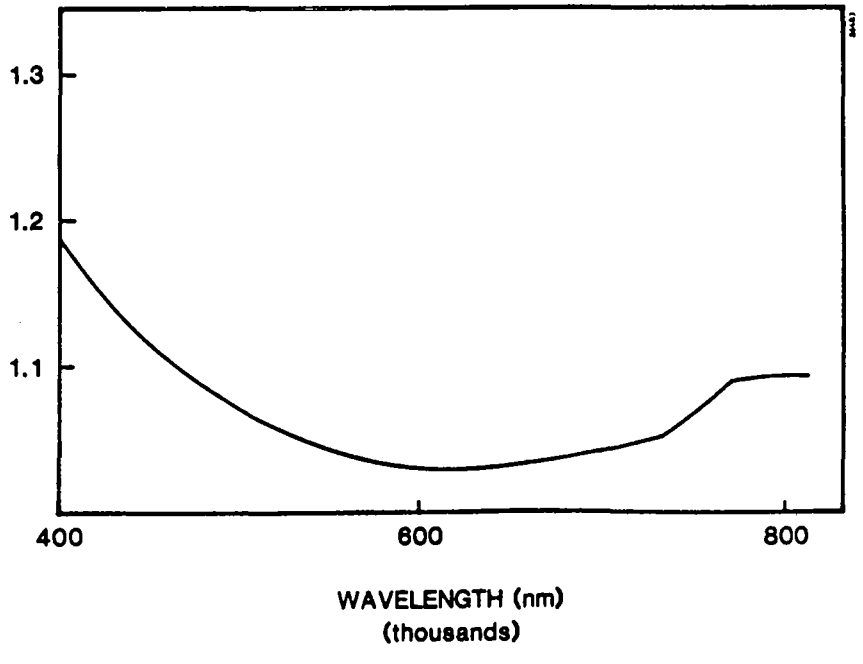

FIGURE 2-1. QE(-1V)/QE(0V) RATIO FOR CELL No. 30008-D7.

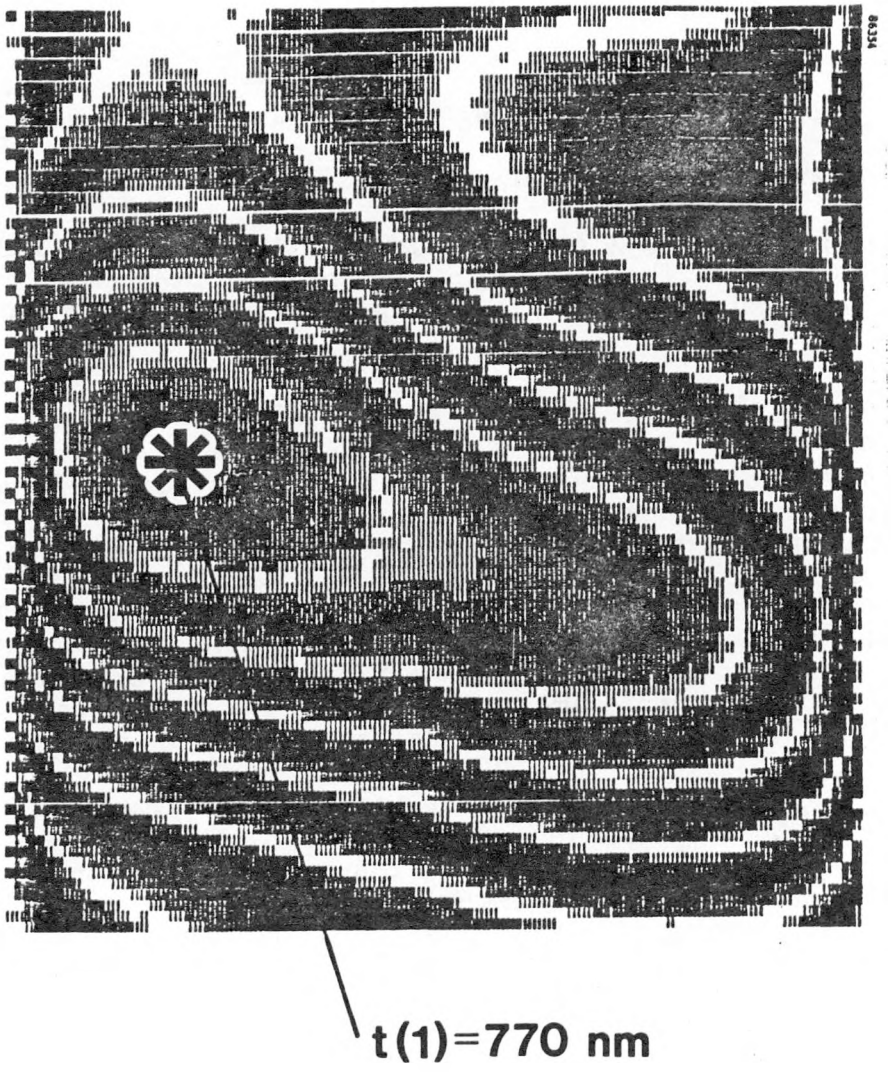

FIGURE 2-2. REFLECTANCE SCANNING PATTERN FOR a-Si:H SAMPLE 30025A.

SECTION 3

NON-SEMICONDUCTOR MATERIAL RESEARCH

3.1 DEPOSITION OF SnO_2:F

The objective of this task is to deposit high-transparency, high-conductivity, textured SnO_2:F films on a glass substrate. We have chosen to use the technique pioneered by R. Gordon of Harvard University,[1] chemical vapor deposition from tetramethyl-tin (TMT).

The basic process and a schematic of the deposition system implemented at Spire have been previously described.[2] The severe safety hazard posed by TMT has been a major concern[3] and our deposition system has been designed to insure containment of the chemical.

3.1.1 Safety

One of the key safety features of our deposition system is the use of a vacuum pump. This pump allows us to deposit the films at low pressure (never shown before). It also has a safety function: purging of the deposition chamber and gas lines more thoroughly than is possible in an all-atmospheric-pressure system. This reduces the exposure risk of personnel to residual TMT when loading and unloading the process chamber. The use of a vacuum pump requires two pressure control valves, one to maintain the pressure inside the bubbler at a fixed value (so that the concentration of TMT in nitrogen can be fixed) and the second to maintain a steady pressure in the chamber. The chamber pressure is usually maintained at 600 torr so that any leaks which may develop will tend to contain TMT.

Additional safety measures include a decomposition furnace (typically 1200°F) between the chamber or bypass line and the vacuum pump to insure that all TMT is oxidized to SnO_2. Filters before and after the vacuum pump trap particulates, protect the pump, and reduce harmful emissions into the atmosphere through oil mist. The pump oil is Fomblin* because standard hydrocarbon oil will explode when pumping gas with high oxygen concentrations, and because the freon vapor used to dope the films (CF_3Br) dissolves hydrocarbon oil as fast as any other known solvent. The bubbler, gas controls, reactor and decomposition furnace are inside a vented cabinet which provides full secondary containment of toxic material. The loading/unloading port of the reactor, which is sealed during operation, is also inside the vented cabinet. In the event of a power failure, the blower for the vented cabinet is run by an emergency power supply, and residual gas in the chamber can be purged by high-pressure nitrogen flow passing through the decomposition furnace (which has a high thermal mass) before exhausting to atmosphere. An automated gas detection system (Telos) monitors the TMT level in the vented cabinet and room air. No leaks have been found to date.

3.1.2 Operation of Deposition System

Full operation of the deposition system was initiated in October, but the internal heater was inadequate. The heater did not reach design temperature and the insulating feet attached left too much dust in the chamber, which affected film quality and clogged the

* Fomblin is a Montedison trademark for perfluorinated polyethers (PFPE), grade Y14/6 used in this application furished by Leybold-Heaeus.

pressure-control valve. The heater was redesigned with a welded, rather than bolted-box, construction, allowing the use of a larger heating element. A transformer was used to boost the voltage available to power the internal heater, and additional strip heaters were placed on the top and bottom surfaces of the chamber, which were insulated. Stainless steel wheels replaced the insulating legs to cut down dust formation.

The new heater was tested at the end of February. The temperature of a sample, measured using melting laquers (from Omega Engineering, Inc.), was between 593°C and 621°C over the entire glass substrate when the thermocouple reading was 352°C. The thermocouple is in contact with an internal plate near the extreme back of the heater where electrical connections exist; the desired temperature at this point is lower than at the sample, for the wire insulation is only rated to 500°C. Most deposition runs are at 352°C reading on this thermocouple, insuring a sample temperature of over 600°C. The thermal uniformity of the heater was also measured, in open air, using an infrared imaging camera. The temperature variation on a glass sample was $\pm$2°C from edge to edge, and better than $\pm$1°C over 90% of the sample at an average temperature of 160°C. At higher temperatures in the enclosed chamber, the percent variation in sample temperature should be reduced.

The first two months (March, April) of work in depositing tin-oxide layers broadly investigated the effect of the following parameters: (a) nitrogen/oxygen ratio varied from 5:1 to 1:5, (b) freon concentration varied from 1 to 10% of total gas flow, (c) total gas flow varied from 1 to 5 standard liters per minute (slpm), (d) TMT concentration varied from 0.1% to 0.5% of total gas flow, and (e) the speed of translation of the heater under the nozzle was varied from 1 to 20 cm/minute. The following parameter were held fixed: (a) chamber pressure was approximately 600 torr (some run-to-run variation but very steady during deposition), (b) TMT bubbler held at 10°C and 700 torr pressure, and (c) sample temperature believed to exceed 600°C in all cases. The thermocouple readings were monitored, with the calibration to sample temperature previously described. All samples were cleaned, Number 7059 glass by Corning (low sodium glass).

The uniformity of all of these early films was obviously affected by the nozzle design. With a minimum reproducible nozzle gap of 0.05 mm, which might change when the nozzle is indirectly heated, the gas flow was not uniform across the nozzle width. The nozzle design is still being studied.

3.1.3 SnO_2:F Film Quality

Several SnO_2:F films were deposited on Corning 7059 glass, defining the parameter space for specular and textured films with sheet resistances $R\square < 50\ \Omega/\square$. Specular and textured films were obtained for low and high O_2 flow rates, respectively. Process and quality parameters of representative samples are shown in Table 3-1. The film quality is expressed by the factor:

$$M = \text{Conductivity/Absorptivity}$$

which for high-quality films can be approximated by:

$$M = -1/[R_\square \times \ln(1-A)]$$

where A is the absorptance, obtained from reflectance R and transmittance T using A = 1 -(R+T). The value of M is independent of film thickness. We have not yet developed an accurate method for measuring A in textured samples and its values are not reported for Sample SN0006.

TABLE 3-1. PROCESS AND QUALITY PARAMETERS OF SnO_2:F FILMS

SAMPLE	N_2 (%)	O_2 (%)	CF_3Br (%)	TMT (%)	R□ (Ω/□)	Absorptance (500-800 nm) (%)	M	Type
SN0006	40.0	50.0	10.0	0.2	10-20	---	---	Textured
SN0013	80.5	15.0	4.3	0.2	22-25	1-2	3.3-3.7	Specular
SN0015	80.5	15.0	4.3	0.2	11-20	4.0	1.2-2.2	Specular

Note that Sample SN0013, part of which was forwarded to SERI, had a value of M that, in some areas, exceeded all values initially reported by the Harvard group. Its optical characteristics can be seen in Figure 3-1.

Textured films were deposited at high oxygen concentrations. These films were all non-uniform, with the texture varying between the front and back of the sample. The non-uniformity is believed to be related to nucleation of SnO_2 on a clean glass surface, and future experiments are planned to test the growth of a textured tin-oxide layer deposited on top of a thin specular layer of tin-oxide. Examination of textured films in a scanning electron microscope (SEM), Figure 3-2, showed that the average feature size of these films (a) was about 500 nm with widely scattered grains about 1500 nm in size (b). The back-scattering image (c) shows a uniform composition, and few defects are seen at lower magnification (d). This SEM was also used to look for fluorine content by EDS. However, none was detected against the tin and silicon background.

With improved uniformity, the SnO_2 films deposited in this reactor to date can meet all of the specifications for this program.

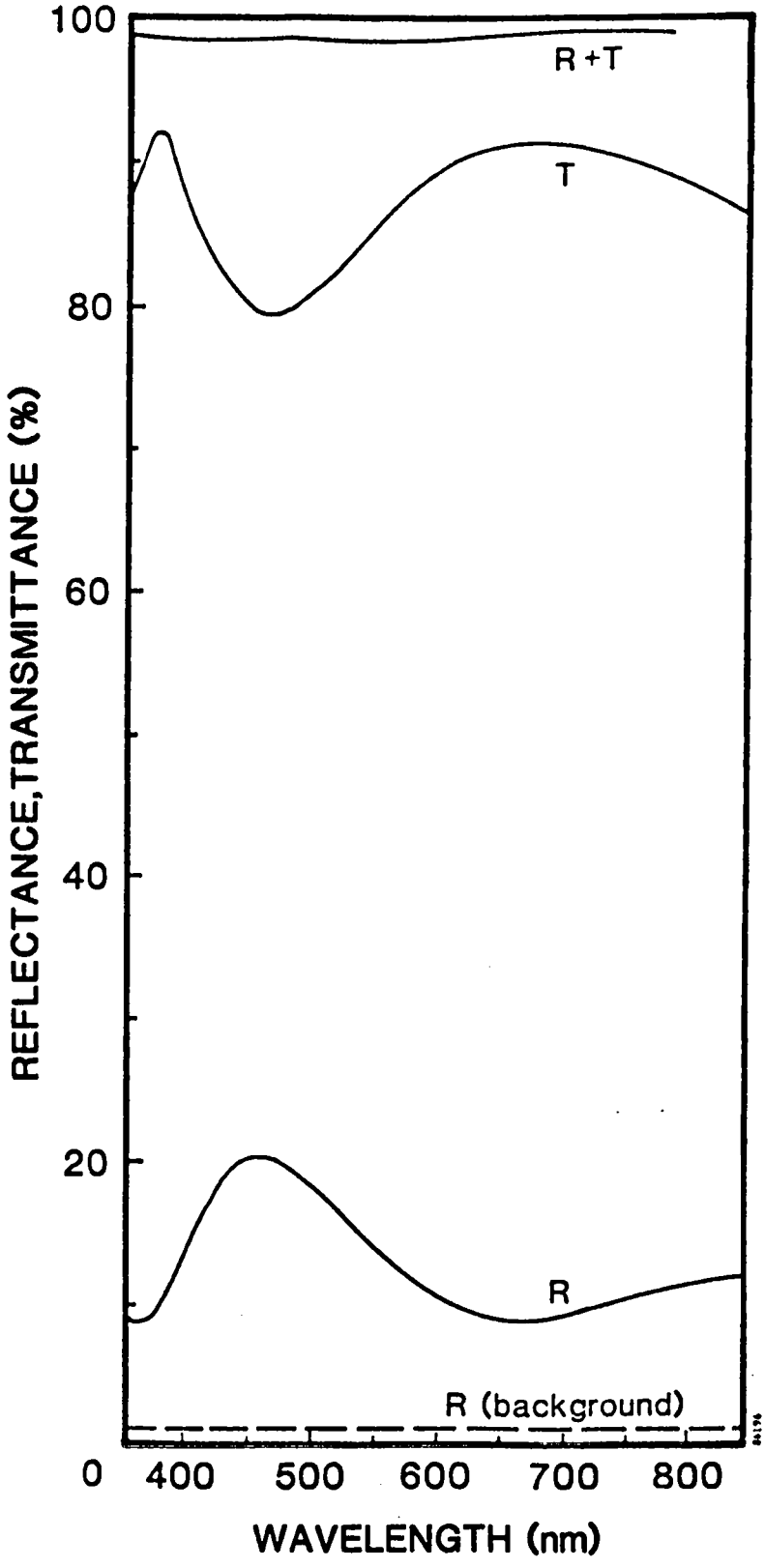

FIGURE 3-1. OPTICAL CHARACTERISTICS OF SnO_2:F FILM, Sample SN0013.

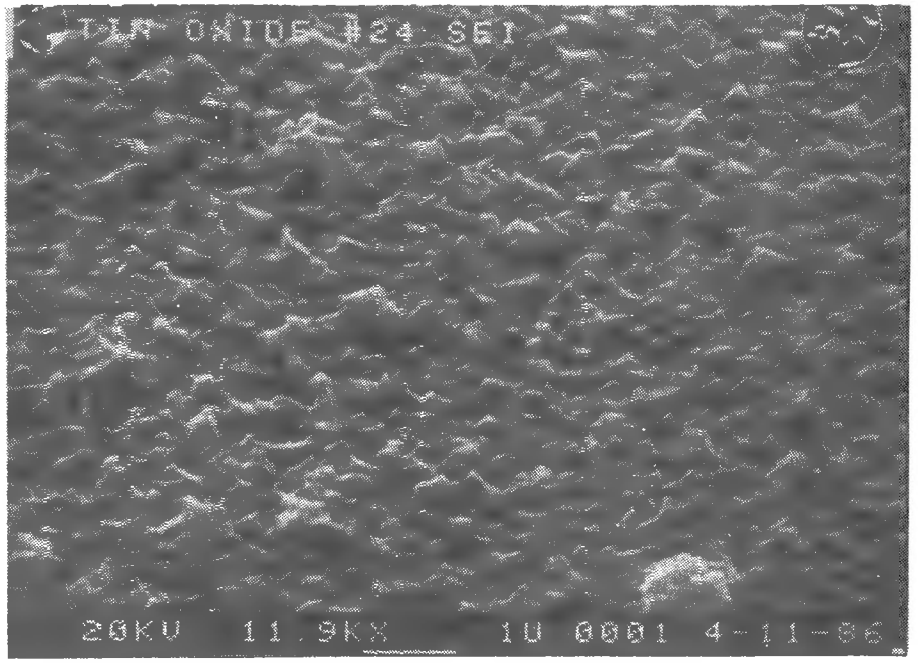

a) 11900x Magnification, feature height 500 nm

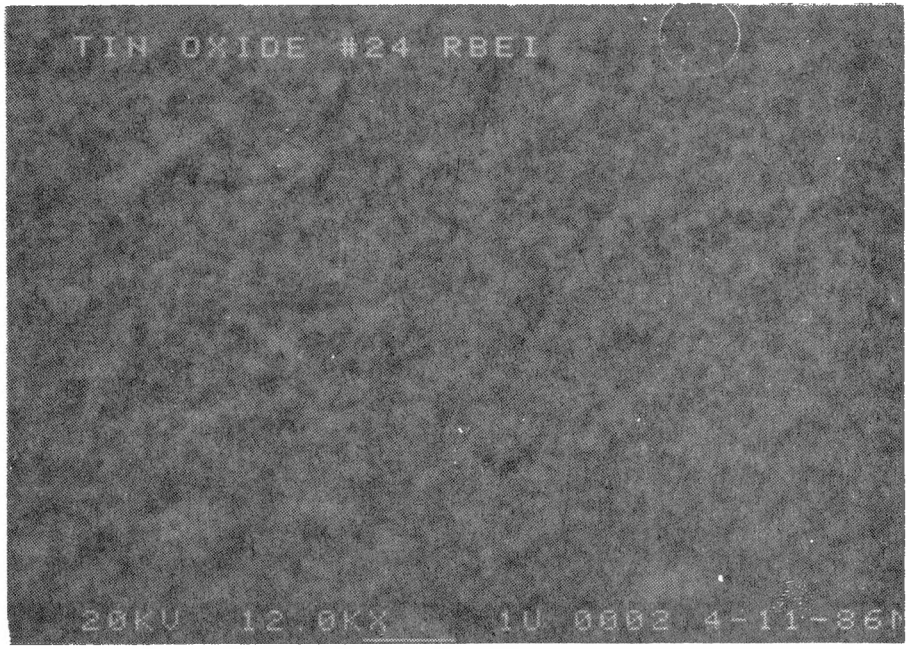

c) Robinson backscattered electron image of figure (a)

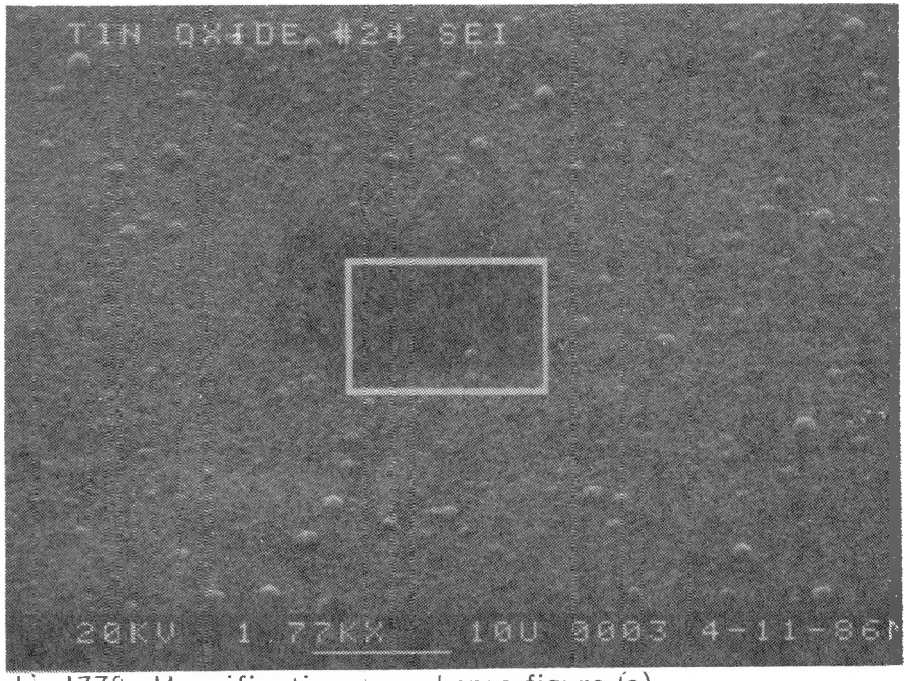

b) 1770x Magnification, boxed area figure (a)

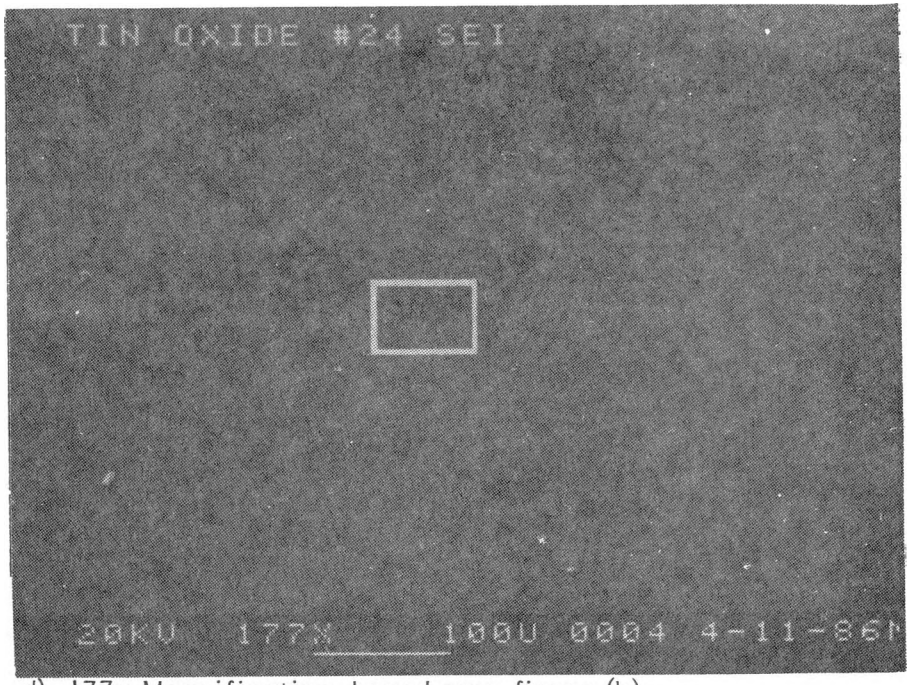

d) 177x Magnification, boxed area figure (b)

SECTION 4

SINGLE JUNCTION CELL RESEARCH

4.1 a-Si:H CELLS

The main effort has been directed at optimizing the performance of a-Si:H cells for use as the top cell in a tandem device. Also, a-Si:H devices, because of their higher reproducibility, as compared with a-(Si,Ge):H devices, can be used to evaluate the effectiveness of design changes such as those relating to photon optimization. Therefore, the focus of this work has been on three areas:

1. High efficiency a-Si:H cells, including high-bandgap cells.
2. High-reflectance back contacts.
3. Textured SnO2:F/glass superstrates.

We have been unable to avoid B contamination at the p-i interface of devices made in the single-chamber reactor (Reactor 1) without, at the same time, radically extending the total deposition time.[2] Therefore, the majority of devices in this work have been made in our multi-sector reactor (Reactor 2)*, with Reactor 1 dedicated to the development of optimum films for the device effort.

4.1.1 Device Fabrication in Multi-Sector Reactor

No major changes have been introduced in the fabrication process. The key features of our standard fabrication technique are:

1. SiH_4 plasma cleaning before p^+-layer growth for control of P and atmospheric contamination of the p^+-layer.

2. High-conductivity, highly transparent a-(Si,C):H p^+-layers leading to high V_{OC} and low J_{SC} losses.

3. SiH_4 plasma cleaning after p^+-layer growth for control of B contamination of the i-layer.

4. Graded band gap i-layer in a-Si:H cells to minimze back-diffusion of electrons from the i-layer to the p^+-layer.

Processes 1) and 3) are essential for obtaining high-efficiency devices but are very time consuming. We will study alternative ways of controlling contamination.

In order to increase E_g, several techniques have been successfully used. Generally, use of lower substrate temperatures and higher $[H_2]/[SiH_4 + H_2]$ ratios yields higher E_g values.[2] Typical process conditions for high-efficiency a-Si:H cells are summarized in Table 4-1 for both lower and higher E_g cells, a-(Si,Ge) i-layers will be discussed in Section 4.2.

* Samples made in reactors 1 and 2 have serial numbers starting with 1 and 2, respectively.

4.1.2 High Efficiency a-Si:H Cells

Two a-Si:H cells with efficiencies in excess of 9% under a 100 mW/cm^2, AM1.5 solar simulator and 0.1 cm^2 area were made during this period. Several other 0.1 cm^2 cells showed efficiency of over 8%. A summary of the highest efficiency cells measured in each of twelve runs can be seen in Table 4-2. Only the highest efficiency cell in each run is reported in this table.

The I-V characteristic of cell 20319-C8 is shown in Figure 4-1. The ratio QE(-1V)/QE (0V) for this cell exhibits the low values typical of high efficiency cells in the wavelength range $\lesssim$ 550 nm (Figure 4-2).

4.1.3 High Band Gap a-Si:H Cell

The key purpose of a-Si:H cell optimization in this program is to use such a cell as the top cell in a tandem structure. In this application, it is important for the top cell to have a relatively high band gap. All our high-efficiency cells fulfill this condition, as compared to other reported high-efficiency cells having $E_g < 1.75$ eV.[4] We will, however, arbitrarily draw a distinction between low and high bandgap at 1.80 eV and separately report three cells with $E_g \gtrsim 1.80$ eV in Table 4-3. These cells generally had lower light-generated current but exhibited V_{oc} and FF comparable to lower gap cells.

4.1.4 Effect of SnO_2:F Texture on a-Si:H Cell Efficiency

One of the key elements in achieving high efficiency is the SnO_2:F texture. All the cells reported above have been grown on commercially obtained textured superstrates. In the past, however, we have experienced problems in achieving a steady supply of textured SnO_2:F, and this has led to inconsistency in cell performance.

During this period we have completed the development of our SnO_2:F CVD reactor and compared the effects of the various degrees of texture achievable in our own films on cell efficiency.

Two half substrates (50 cm^2 each), one textured and one untextured, were used in the fabrication of a-Si:H devices. The I-V parameters of the highest efficiency devices in each half are given in Table 4-4.

The quantum efficiencies of the two devices in Table 4-4 and their ratio can be seen in Figures 4-3 and 4-4. Integration of the difference of the measured quantum efficiencies with an AM1 spectrum yields a J_{sc} difference of 0.6 mA/cm^2. The enhancement due to texture is thus 5-8%. This increase is smaller than expected, although crucial to achieving high efficiencies.

From the above, plus the data in Section 3, we conclude that our CVD reactor can provide SnO_2:F of adequate quality, thus contributing to repeatability of our high efficiency a-Si:H process.

TABLE 4-1. TYPICAL PREPARATION PARAMETERS FOR a-Si:H CELLS.

1. p^+-layer

Dopant Gas: 2% B_2H_6 in He.

Total Flow = 52.5 sccm

$[B_2H_6/[SiH_4 + CH_4 + H_2 + B_2H_6 + He] = 0.36\%$

$[CH_4]/[SiH_4 + Ch_4 + H_2 + B_2H_6 + He] = 27\%$

$[SiH_4]/[SiH_4 + CH_4 + H_2\ B_2H_6 + He] = 36\%$

$[H_2]/[SiH_4 + CH_4\ H_2\ B_2H_6 + He] = 18\%$

T = 220°C

P = 200 mTorr

$V_{substrate} = -10V$

Power = 120 - 180 mW/cm^2

2. i-layer

Total Flow = 20-75 sccm

$[SiH_4]/[SiH_4 + H_2] = 20\text{-}60\%$

$[H_2]/[SiH_4 + H_2] = 40\text{-}80\%$

T = 275 - 300°C

P = 100 - 200 mTorr

$V_{substrate} = -10V$

Power = 120 - 180 mW/cm^2.

3. n^+-layer

Dopant Gas: 2% PH_3 in Ar

Total Flow = 60 sccm

$[PH_3]/[SiH_4 + H_2 + PH_3] = 6.7\%$

$[SiH_4]/[SiH_4 + H_2 + PH_3] = 33.3\%$

$[H_2]/[SiH_4 + H_2 + PH_3 = 33.3\%$

T = 325 °C

P = 200 mTorr

$V_{substrate} = 0\ V$

Power = 180 mW/cm^2

TABLE 4-2. I-V CHARACTERISTICS OF HIGH EFFICIENCY a-Si:H CELLS (AREA=0.1 cm^2, Al BACK CONTACT)

Sample No.	E_g (eV)	V_{oc} (mV)	J_{sc} (mA/cm^2)	FF (%)	Eff (%)
20319-C8	1.78	867	15.1	69.6	9.1
20363R-B8*	1.78	838	15.3	70.9	9.1
20356-A8	1.79	826	15.4	68.6	8.7
20358-A8	1.78	840	15.5	70.9	8.7
20317-C8	1.79	860	14.2	69.6	8.5
20321-B7	1.78	872	14.1	67.8	8.4
20361-C7	1.79	847	14.1	69.7	8.3
20320-A8	1.77	857	16.2	59.8	8.3
20300-D8	1.79	862	14.0	68.0	8.2
20339-A8	1.77	865	14.6	65.2	8.2
20344-C8	1.79	846	14.4	67.5	8.2
20318-A8	1.78	857	14.7	63.0	8.0

*Cell 20363-B8 was fabricated on our own SnO_2:F superstrate (See Section 4.1.4).

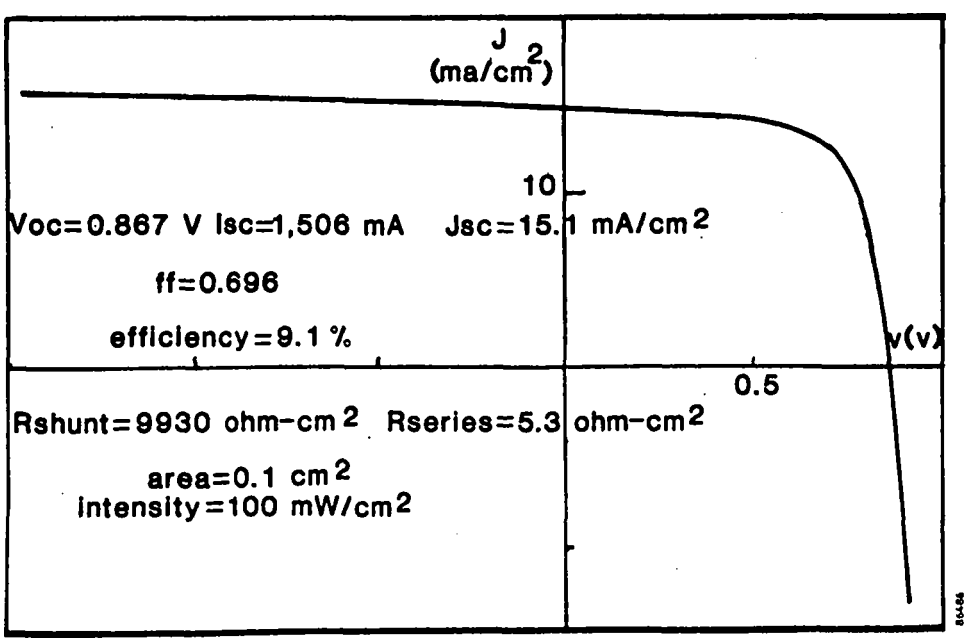

FIGURE 4-1. I-V CHARACTERISTIC OF a-Si:H CELL 20319-C8.

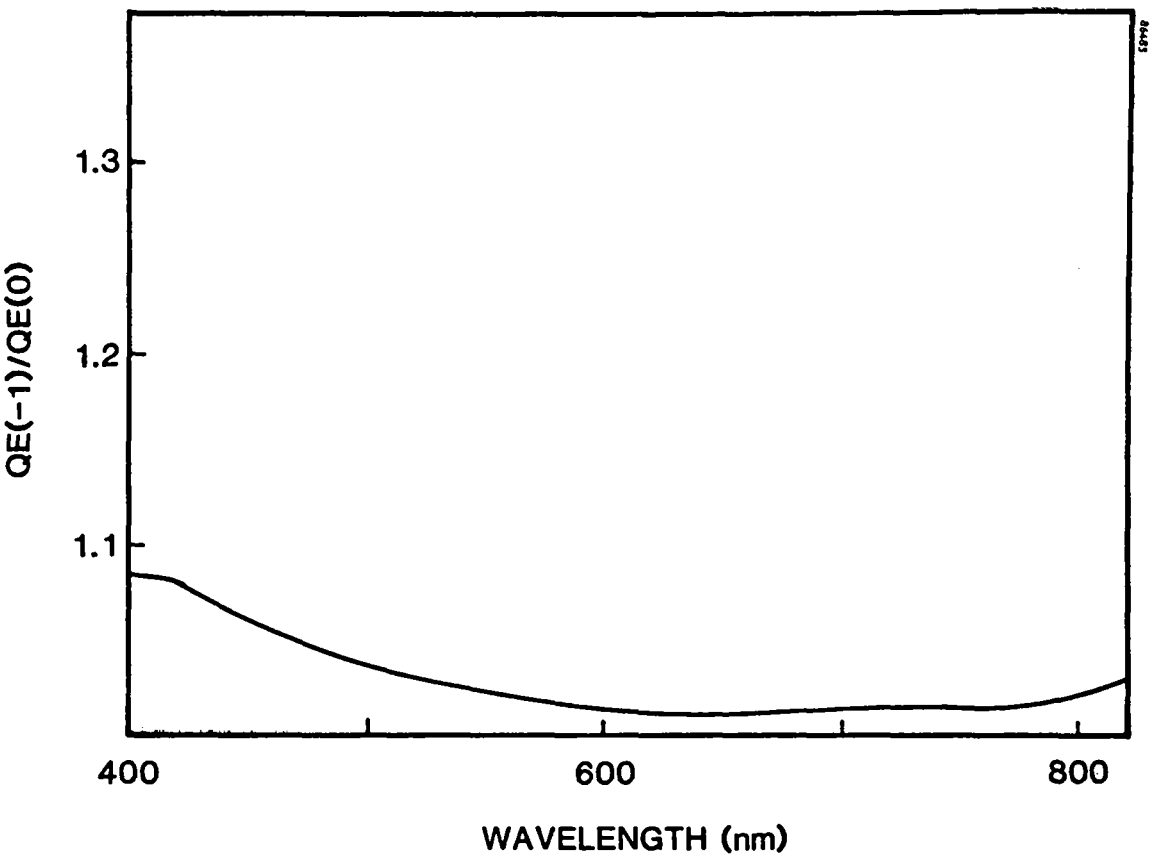

FIGURE 4-2. QUANTUM EFFICIENCY RATIO FOR CELL 20319-C8.

TABLE 4-3. I-V CHARACTERISTICS OF HIGH EFFICIENCY a-Si:H CELLS WITH $E_g \gtrsim 1.80$ eV. (Area = 0.1 cm^2, Al back contact).

Sample No.	E_g (eV)	V_{oc} (mV)	J_{sc} (mA/cm^2)	FF (%)	Eff (%)
20200-C3	1.81	820	14.4	69.6	8.2
20316-B8	1.80	827	14.3	68.7	8.1
20278-B2	1.81	874	13.3	68.6	8.0

TABLE 4-4. I-V CHARACTERISTICS OF a-Si:H DEVICES FABRICATED ON TEXTURED AND UNTEXTURED SnO_2:F (Area = 0.1 cm^2)

Sample No.	Type	V_{oc} (mV)	J_{sc} (mA/cm^2)	FF (%)	Eff (%)
20363L-B8	Specular	827	14.1	68.6	8.0
20363R-B8	Textured	838	15.3	70.9	9.1

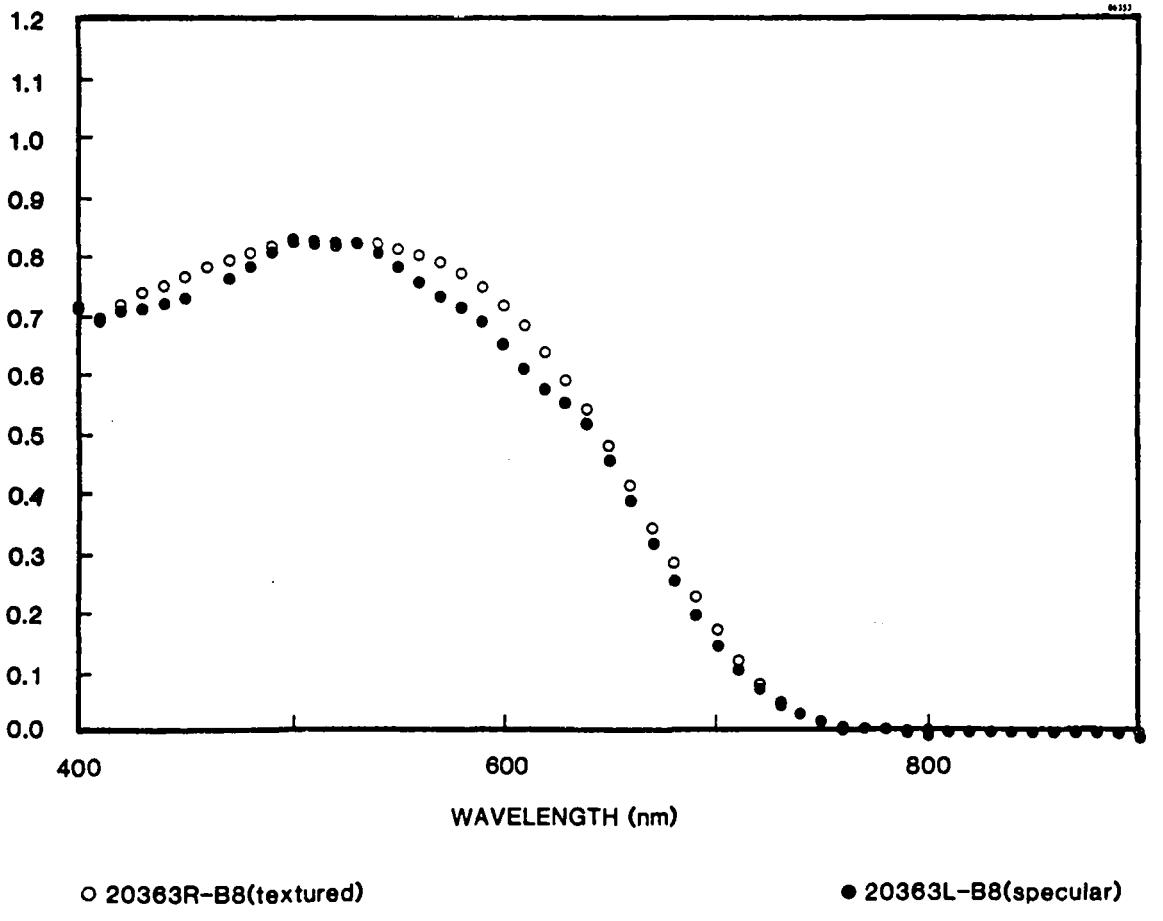

FIGURE 4-3. QUANTUM EFFICIENCIES OF TEXTURED AND SPECULAR a-Si:H DEVICES.

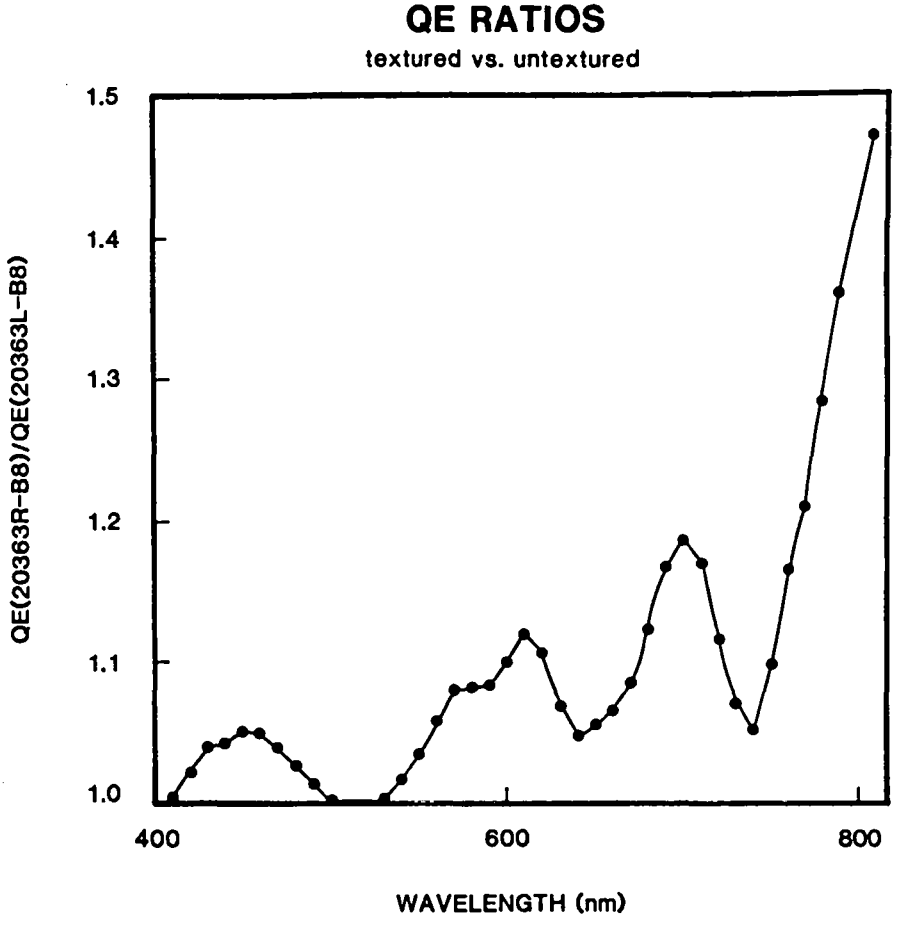

FIGURE 4-4. RATIO OF QUANTUM EFFICIENCY OF CELL 20363R-B8 TO THAT OF 20363L-B8.

4.2 HIGH EFFICIENCY a-(Si,Ge):H CELLS

We have obtained graded band gap a-(Si,Ge):H cells with 7.5% efficiency. The band gap diagram for this device is shown in Figure 4-5. In this approach, the i-layer is smoothly graded from that of a-Si:H to that of a-(Si,Ge):H by varying the GeH_4 fraction in the gas mixture. It has been shown[5,6] that, as the atomic fraction f[Ge] = [Ge]/[Ge + Si] increases, the electron affinity of the alloy increases and the conduction band moves toward more negative energies, while the valence band remains within 0.1 eV of its original position. This results in an increased drift field aiding electron transport in the graded region.

Our analysis of this type of device is still qualitative and under development. We believe that the graded band gap structure provides advantages over more conventional single-junction cells with a constant composition a-(Si,Ge):H i-layer. They derive from the lower mobility-lifetime product for electron and hole transport that is generally observed in a-(Si,Ge):H with $E_g \lesssim 1.5$ eV:

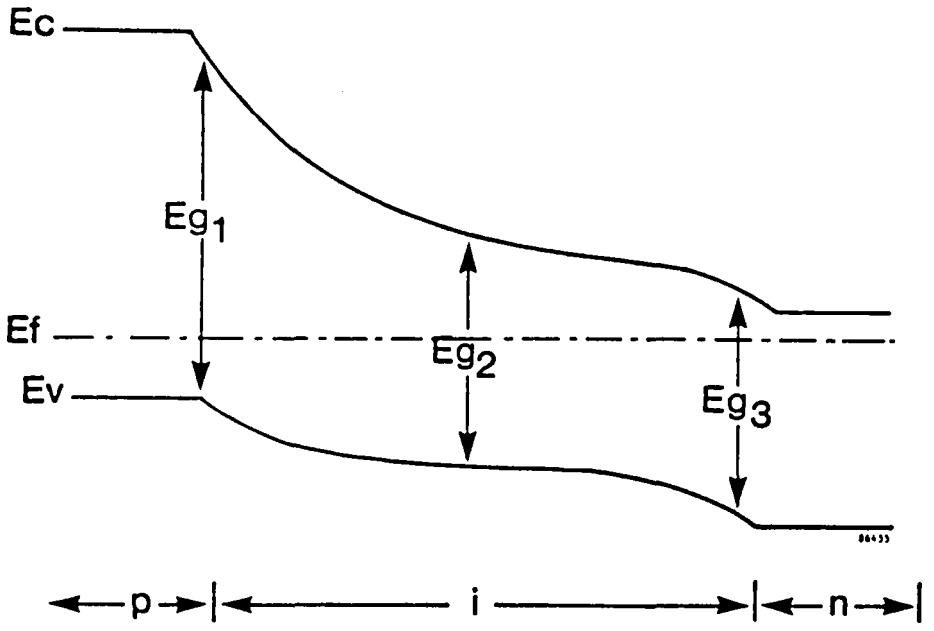

FIGURE 4-5. BAND-DIAGRAM OF p-i-n GRADED BAND GAP a(Si,Ge) CELL.

1) Higher V_{OC}, due to reduced recombination in the higher quality a-(Si,C):H region near the p^+-i interface.

2) Higher FF due to the enhanced electron transport caused by the conduction band grading and the resulting increase in the drift-field.

3) Increased QE in the wavelength region $\gtrsim$ 600 nm due to improved hole transport through the lower [Ge]/[Si + Ge] region of the i-layer.

We are unable at present to model exactly the carrier generation in order to predict the values of J_{SC} that can be attained with a given E_g and grading profile of the a-(Si,Ge):H i-layer. To properly use this a-(Si,Ge):H cell as the bottom cell in a tandem structure, the improvement in the hole collection efficiency induced by the addition of the high quality, low f[Ge] portion of the i-layer, needs to exceed the decrease in carrier generation due to the higher band gap of this material. This seems, in the absence of a quantitative model, to be qualitatively possible, since the decrease in carrier generation in question will occur in a spectral region already depleted of photons by the top cell of the structure.

The information that follows is meant to support this plausibility argument. Preliminary experiments on the application of this technique to practical tandem structures will be presented in Section 5. The question of the bandgap of the high f[Ge] material will be discussed in Section 4.2.3.

4.2.1 Deposition Conditions for the a-(Si,Ge):H i-layer

Typical deposition conditions for the a-(Si,Ge) i-layer, including the gas flows $Q[SiH_4]$, $Q[GeH_4]$ and $Q[H_2]$, are given in Table 4-5 for the a(Si):H, graded and Ge rich regions of the i-layer.

TABLE 4-5. DEPOSITION CONDITIONS FOR a-(Si,Ge):H i-LAYER OF GRADED BAND GAP CELL

Region	$Q[SiH_4]$ (sccm)	$Q[GeH_4]$ (sccm)	$Q[H_2]$ (sccm)	T (°C)	P (mTorr)	$V_{substr.}$ (V)	Power (mW/cm^2)	Time (min.)
a-Si:H	20	0	0	325	200	-10	100	5
Graded a-(Si,Ge)	20	0-1.5	0-53.5	325-270	200	-10	100	90
Maximum [Ge]/[Si]	15	1.5	53.5	270	200	-10	100	60

4.2.2 I-V Characteristics of a-(Si,Ge):H Cells

The I-V characteristics and quantum efficiency at -1 and 0 V for the highest efficiency a-(Si,Ge):H cell made in this period are shown in Figures 4-6 and 4-7. For comparison, we show the same type of data for cell 20226-B1, having an ungraded i-layer made under similar plasma-process conditions (Figures 4-8 and 4-9). The improved FF and QE(-1V)/QE(0V) ratio for the graded cell support the above model.

The I-V characteristics of several graded a-(Si,Ge):H cells with efficiencies exceeding 6.5% are reported in Table 4-6. The values of band gap denoted by E_g(QE) have been determined from QE data by comparison to the QE of an a-Si:H p-i-n device of known band gap. Their meaning for a graded band gap device needs to be clarified by more careful optical modeling. They are only reported and used here as a measure of the displacement of the cell response in the near-infrared wavelength region as the values of [Ge]/([Ge] + [Si]) in the i-layer are varied. The question of the true value of E_g in the high Ge content region will be addressed below.

One substrate (20277) containing a number of cells was sent to SERI to confirm the efficiency measurements. Table 4-7 shows the results obtained at Spire and at SERI.

The results verify the attainments of a 7% efficiency on 0.1 cm^2 devices. Almost that efficiency was measured on a 0.5 cm^2 device. As we can see from the data, this technique can yield FF > 55% with J_{SC} > 15 mA/cm^2, which is not easily obtainable with ungraded i-layers.

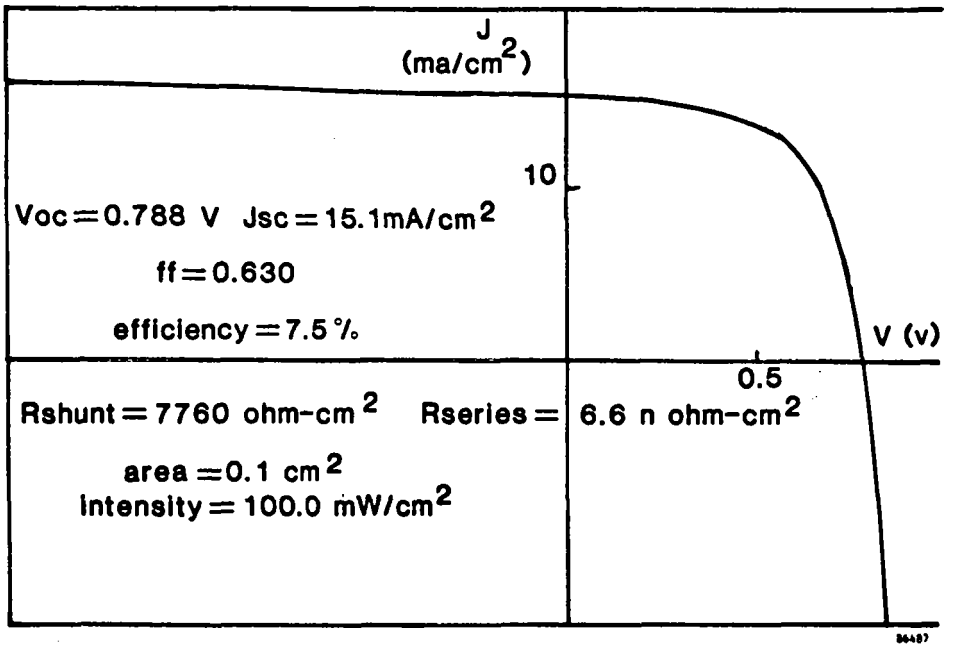

FIGURE 4-6. I-V CHARACTERISTICS OF a-(Si,Ge):H CELL 20276-B5.

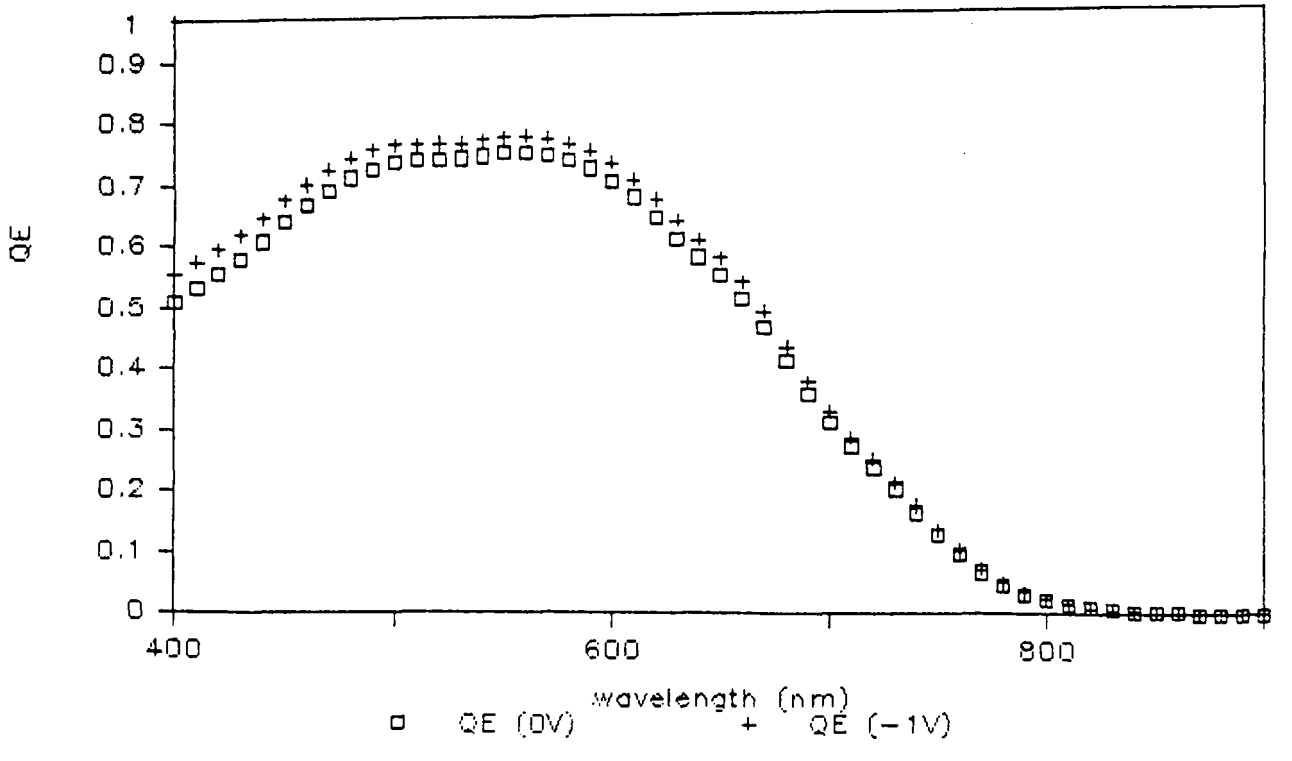

FIGURE 4-7. QUANTUM EFFICIENCY OF GRADED BAND GAP a-(Si,Ge):H CELL 20276-B5.

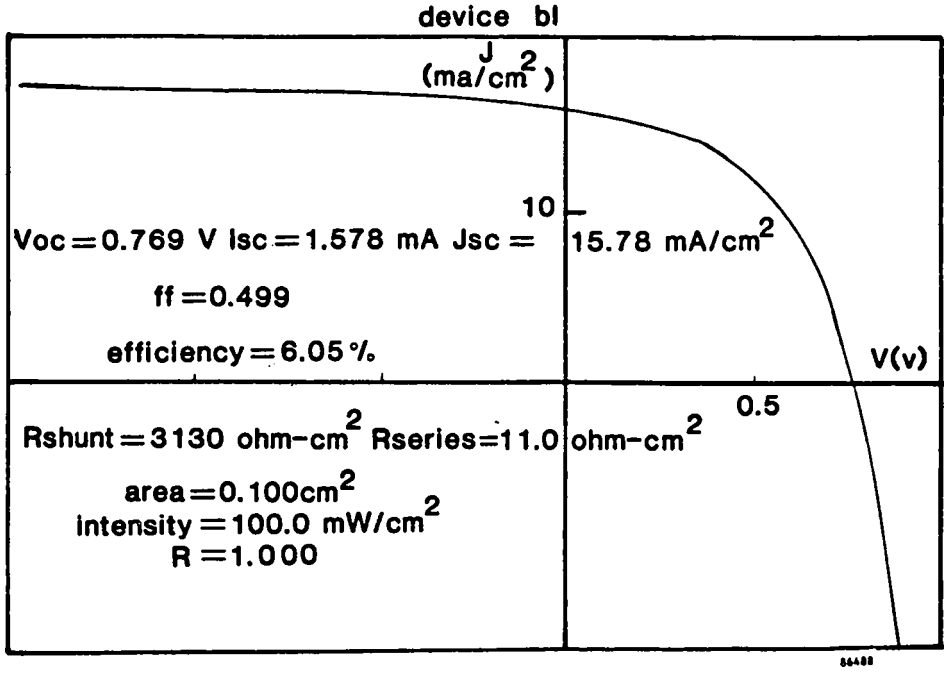

FIGURE 4-8. I-V CHARACTERISTICS OF a-(Si,Ge):H CELL 20226-B1.

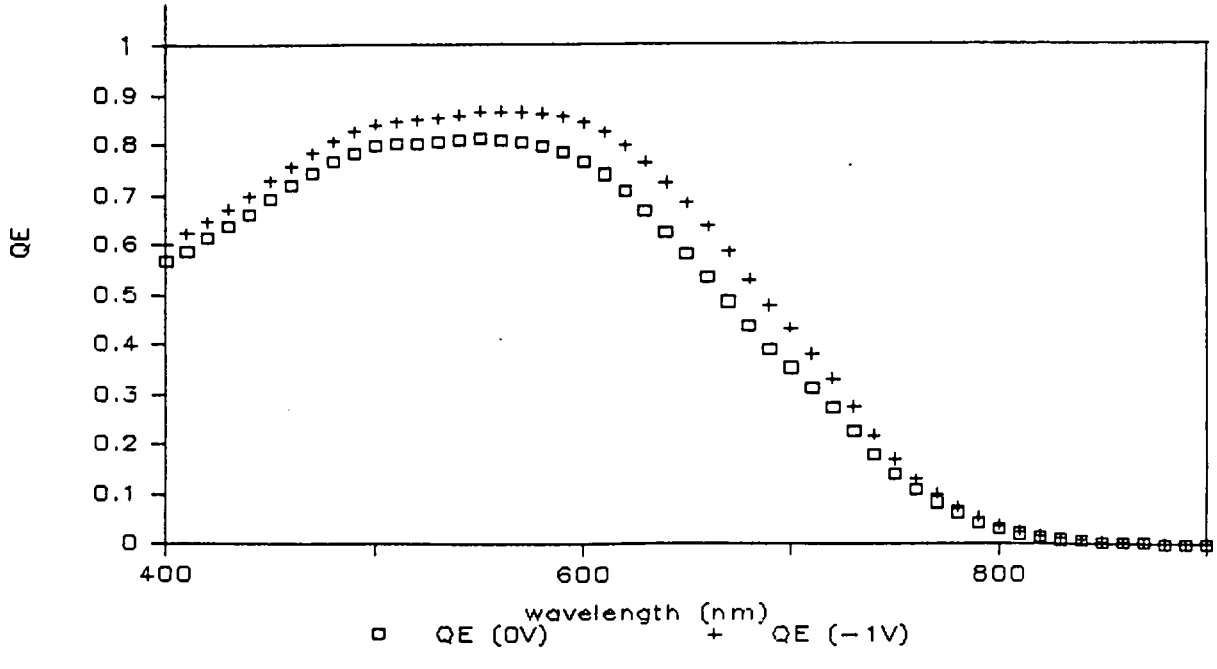

FIGURE 4-9. QUANTUM EFFICIENCY OF UNGRADED a-(Si,Ge):H CELL 20226-B1.

TABLE 4-6. I-V CHARACTERISTICS OF HIGH-EFFICIENCY, GRADED BAND GAP a-Si:H CELLS WITH $E_g(QE) \gtrsim 1.70$ eV

Sample No.	$E_g(QE)$ (eV)	V_{oc} (mV)	J_{sc} (mA/cm^2)	FF (%)	Eff (%)
20255-B3	1.68	805	14.8	55.2	6.6
20263-C6	1.68	794	14.9	56.4	6.7
20273-A8	1.68	726	15.3	60.5	6.7
20276-B5	1.67	788	15.1	63.0	7.5
20277-C1	1.64	759	15.4	59.6	7.0
20279-B2	1.65	785	13.9	60.9	6.7
20282-B1	1.67	810	15.3	59.2	7.3

TABLE 4-7. I-V CHARACTERISTICS OF CELLS FROM SAMPLE 20277

Sample Test	Date	V_{oc} (mV)	J_{sc} (mA/cm^2)	FF (%)	Eff. (%)	Area cm^2
20277-C1 SPIRE	2/06/86	759	15.4	59.6	7.0	0.100
20277-D7 SPIRE	3/06/86	746	14.8	60.6	6.7	0.500
20277-C1 SERI	3/17/86	763	15.7	59.4	7.1	0.101
20277-D7 SERI	3/17/86	768	14.8	60.9	6.9	0.505
20277-C1 SPIRE	3/19/86	752	15.1	59.2	6.7	0.100
20277-D7 SPIRE	3/19/86	744	14.6	61.0	6.6	0.500

4.2.3 Auger Analysis of Graded-Band Gap a-(Si,Ge):H Cells

Conditions for growth of the lowest band gap portion of the i-layer in a graded band gap cell obtain when $Q[GeH_4]/Q[SiH_4]$ is a maximum. Sample No. 20275, for example, was grown with a maximum $Q[GeH_4]/Q[SiH_4] = 0.10$, the same as sample 20276, which yielded the highest efficiency cell. The question arises as to what is the band gap and the atomic fraction f[Ge] = [Ge]/([Ge] + [Si]) in that region of the i-layer, under the given growth conditions.

AES depth profile data from Sample No. 20275 were obtained for Spire by the Institute of Energy Conversion, Univesity of Delaware, and can be seen in Figure 4-10. The profile is characterized by a broad region with [Ge]/([Ge] + [Si]) = 0.39. Using data by K.W. Mitchell et al.,[7] E_g values of 1.45 to 1.50 eV can be inferred, suggesting that our band gap values are adequately low, at least in the region of the i-layer containing the highest atomic fraction of Ge.

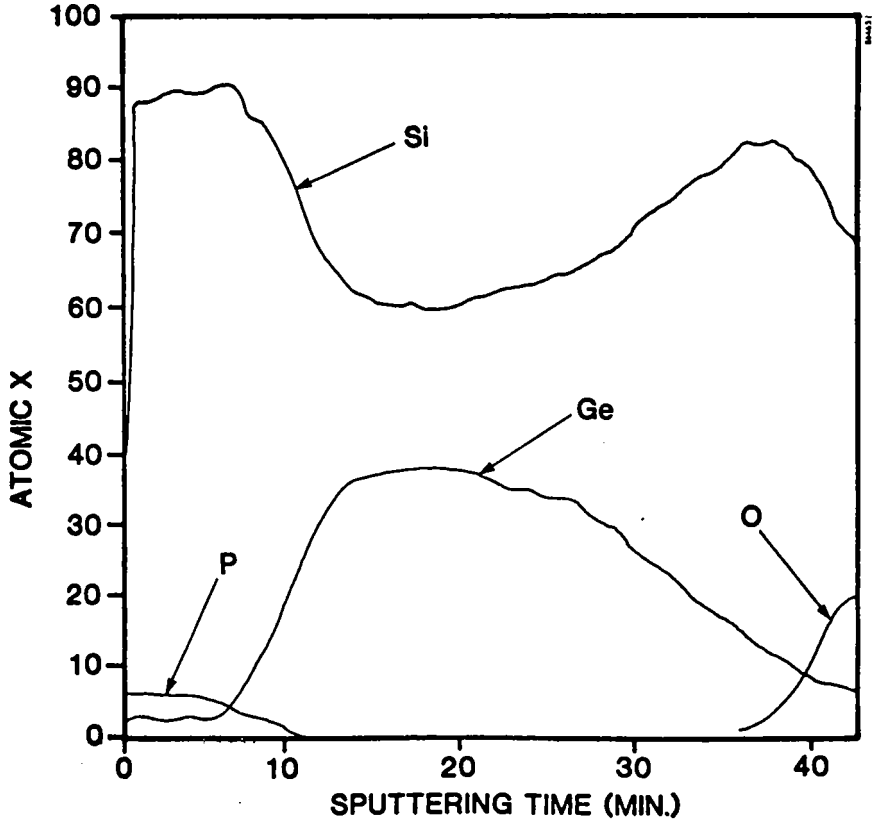

FIGURE 4-10. AES PROFILE OF a-(Si,Ge):H SAMPLE 20275.

4.2.4 Conclusions

As explained in Section 4.2.1, the addition of the Si-rich region to the a-(Si,Ge):H alloy i-layer decreases carrier generation while improving collection. The above results indicate that this approach may yield a suitable optimum, applicable not only to single junction a-(Si,Ge):H devices, but also to their use as a bottom cell in a tandem structure. Improved modelling of the trade-off between generation and collection will be attempted in the remaining period.

4.3 HIGH REFLECTANCE Ti/Ag BACK CONTACTS

Previous efforts had centered on chromium-silver as back contact materials for high contact reflectivity in a-Si:H devices. No acceptable chromium thickness was found that resulted in few device shorts back and sufficient transmission of light to the silver layer. Details of these efforts were presented in the second annual report.

As a consequence, experimental efforts were directed towards the use of titanium-silver back contacts. Initially, very thin Ti layers were deposited (30 Å) and subsequently coated with silver. Even though a quantum efficiency increase of $\geq$ 25% over Al back contacts was measured at 700 nm, substantial device shunting occurred. Because of the latter, thicker Ti deposits (50-100 Å) were investigated. A process was developed that resulted in reflectances in glass/Ti (50 Å)/Ag samples in the 500 to 700 nm range that exceeded 95%. The process for these samples was:

1. Vacuum deposition of a 50 Å Ti layer on 7059 glass.
2. Air anneal at 120° C for 30 minutes and 140° C for 50 minutes.
3. Vacuum deposition of a 5,000 Å Ag layer.

Table 4-8 shows optical data for sample AV17(1).

TABLE 4-8. OPTICAL DATA FOR SAMPLE AV17(1) (λ= 700 nm)

	Glass/TiO_x			Glass/TiO_x/Ag
Comments	R	T	R+T	R_t
Initial	-	0.78	-	-
120°C/30 min.	0.11	0.82	0.93	0.94
140°C/60 min.	0.10	0.85	0.95	0.96

As seen in the table, the reflectance was increased to 96% by the prolonged heat treatment.

Ti/Ag and Al contacts were applied to both a-(Si,Ge):H and a-Si:H cells. After deposition of the Ti contacts, substrates were subjected to the heat treatment described in Section 3 and then followed by Ag vacuum deposition. Textured SnO_2 coated glass substrates were used. Table 4-9 gives the results of these experiments.

TABLE 4-9. I-V CHARACTERISTICS OF a-(Si,Ge):H AND a-Si:H CELLS WITH Ti/Ag AND Al BACK CONTACTS (Area = 0.1 cm^2)

Sample No.	Voc (V)	Jsc (mA/cm^2)	FF (%)	(%)	Contact Type	Comments
20282-A4	799	15.6	54.6	6.8	Ti/Ag	a-Si,Ge:H
20282-A5	794	14.5	57.3	6.6	Al	a-Si,Ge:H
20316-C12	837	14.7	61.5	7.6	Ti/Ag	a-Si:H
20316-C13	840	13.7	63.5	7.3	Al	a-Si:H

For the a-(Si,Ge):H cells, a current density increase of 7.6% is measured in the Ti/Ag back contact cell. For the a-Si:H cells, the increase is 7.3%. In both substrates, a decrease in fill factor was noted. The cause of this decrease is being investigated.

Figure 4-11 shows the quantum efficiency of cells 20316-C12 and 20316-C13. A significant increase in quantum efficiency for the cell with the Ti/Ag back contact is seen at wavelengths greater than 550 nm, as would be expected. The origin of the differences at shorter wavelengths is not immediately apparent, but these are clearly less than at longer wavelengths. Consequently, most of the current density increase is due to the more highly reflecting Ti/Ag back contact.

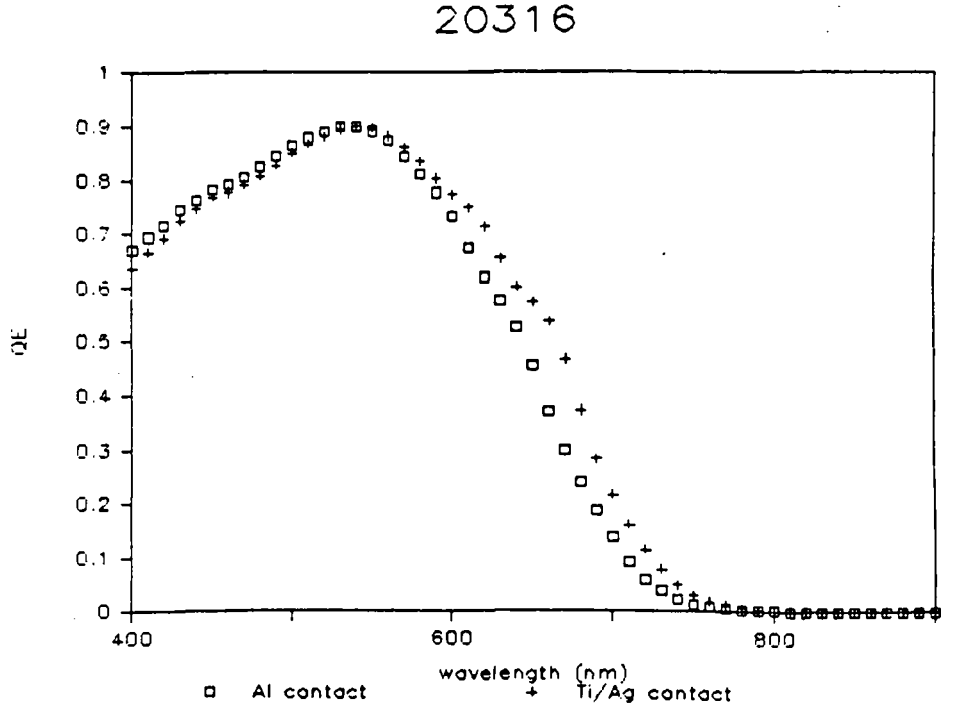

FIGURE 4-11. QUANTUM EFFICIENCY OF CELLS 20316-C12 (Ti/Ag BACK CONTACT) and 20316-C13 (Al BACK CONTACT).

Although a process has been established to obtain highly reflecting back contacts, further work is planned to simplify the process and to determine if Ti/Ag contacts influence the cell fill factors.

SECTION 5

TANDEM JUNCTION CELL RESEARCH

5.1 CELL RESULTS

As a consequence of the efforts on both a-Si:H and a-Si,Ge:H single-junction cells, a small number of substrates containing tandem cells were fabricated incorporating features of the successful single junction cells. Table 5-1 lists the results of the best a-Si:H/a-Si:H and a-Si:H/a-Si,Ge:H cells. Cell area is 0.1 cm^2. Estmatesof the top and bottom cell bandgaps from quantum efficiency data are subject to considerable error and will not be cited here.

TABLE 5-1. I-V CHARACTERISTICS OF BEST TANDEM CELLS FOR SPECIFIED SUBSTRATE

SUBSTRATE/CELL	V_{OC} (V)	J_{SC} (mA/cm^2)	FF (%)	Eff (%)
A. a-Si:H/a-Si:H				
20324/B5	1.637	6.7	67.2	7.4
20309/A7	1.661	5.9	66.0	6.5
20303/C1	1.557	6.4	60.5	6.1
20326/A7	1.616	6.3	66.4	5.8
20285/A3	1.630	5.1	66.8	5.5
20311/B8	1.661	5.9	68.4	5.5
B. a-Si:H/a-Si,Ge:H				
20266/A8	1.586	6.5	69.4	7.2
20283/B5	1.540	6.9	62.6	6.7
20290/B7	1.568	6.3	66.0	6.5
20268/A8	1.531	6.0	66.1	6.1
20228/B1	1.531	6.2	62.8	5.9
20280/C5	1.528	5.7	64.1	5.6

Typical deposition conditions for the tandem cells were as indicated for the individual cells described in previous sections.

On the basis of calculations and prior experience, the 0.1 μm top-cell amorphous silicon layers should be capable of producing short circuit current densities near 7 mA/cm^2 when using specular SnO_2 glass. As seen in Table 5-1, the best cells produce light generated current densities near this value. Cells with lower currents are limited by the output characteristics of the bottom cell.

Figures 5-1 and 5-2 show the quantum efficiency (QE) of the top and bottom cells of tandem cell 20283/85 at 0 and 0.75 V respectively. (When the tandem cell is at 0.75V and 0V bias, the cell in that tandem structure whose QE is being measured is at 0 V and -.75V, respectively.) For this tandem cell, essentially equal amounts of short circuit current are being produced in the top and bottom cells at 0 volts. The values of the fill factor and open circuit voltage strongly indicate that the n^+, p^+ interface between the top and bottom cells produces a low resistance contact with consequent negligible losses in the tandem device.

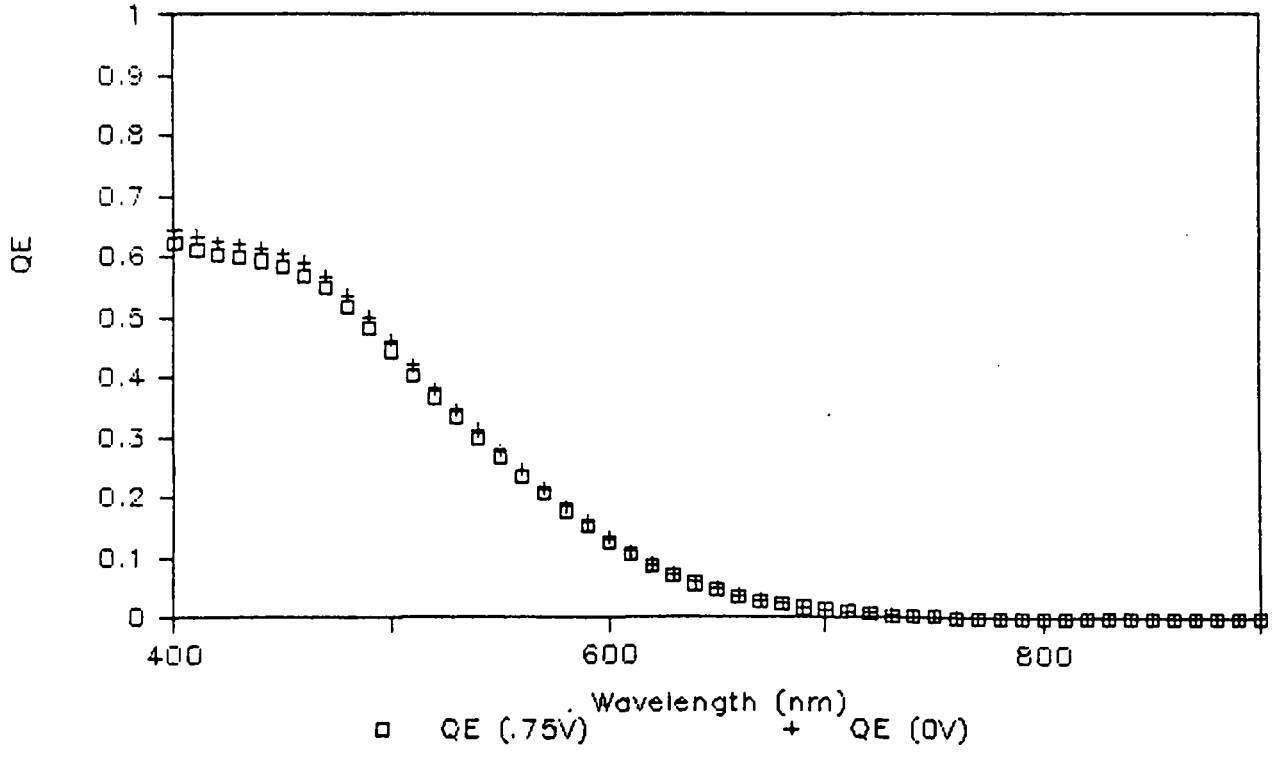

FIGURE 5-1. QUANTUM EFFICIENCY OF TOP a-Si:H CELL AS OBTAINED UNDER RED LIGHT BIAS, CELL #20283RB5.

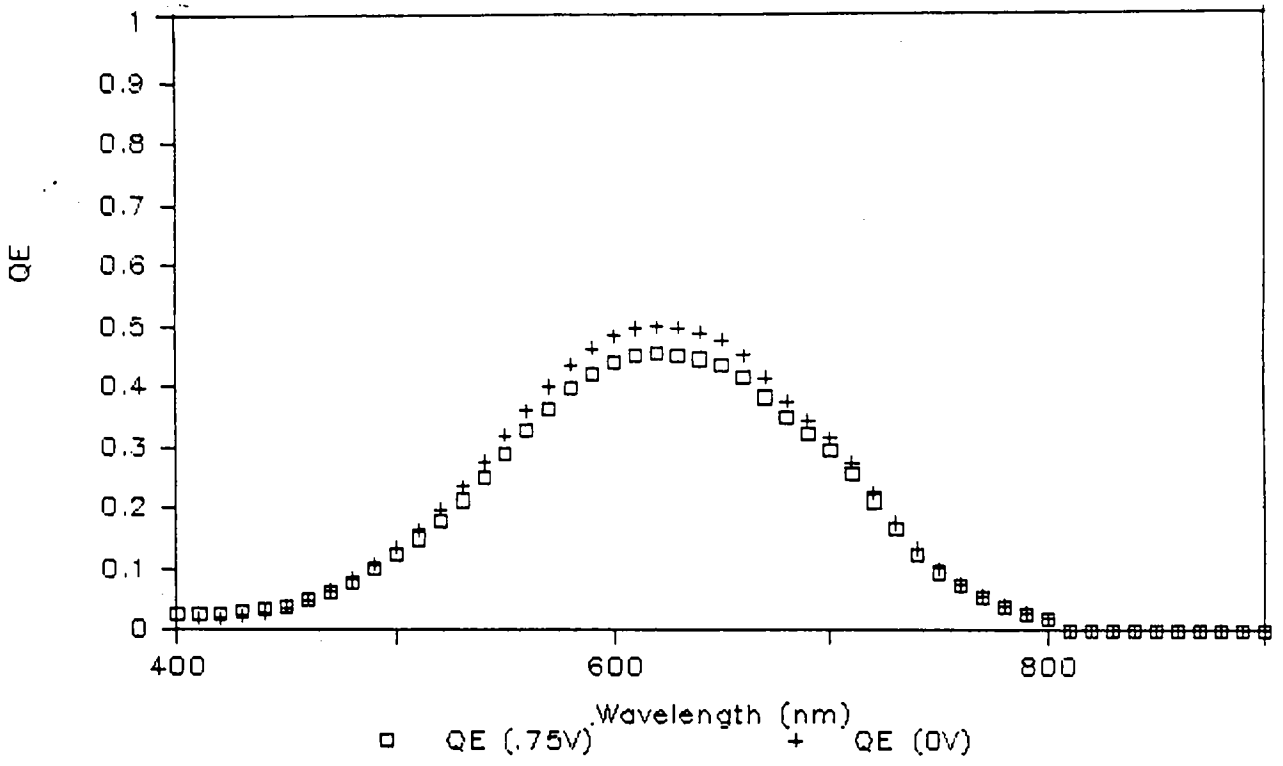

FIGURE 5-2. QUANTUM EFFICIENCY OF BOTTOM a-Si,Ge:H CELL AS OBTAINED UNDER BLUE LIGHT BIAS, CELL #20283BB5.

Test structures having a p-i-n-p configuration have verified that negligible losses are associated with the n-p interface. Figure 5-3 shows the I-V characteristic of such a cell. Note the high fill factor of the cell, which is a strong indication of the ohmic quality of the interface.

From the above tandem cell results, it is clear that efficiency improvements will occur as high performance, low band gap a-Si,Ge:H material is grown and incorporated into tandem devices. For example, as the band gap of the bottom cell is decreased, it becomes possible to use thicker a-Si:H layers in the top cell, thereby increasing the potential current from the individual cells and the tandem cell itself. However, for the combination of band gap and quality available at this time, further improvement in efficiency can be achieved by enhancing the optical absorption in the i-layers of the two cells in the tandem structure; i.e., by using textured tin oxide with lower optical absorption and titanium/silver contacts.

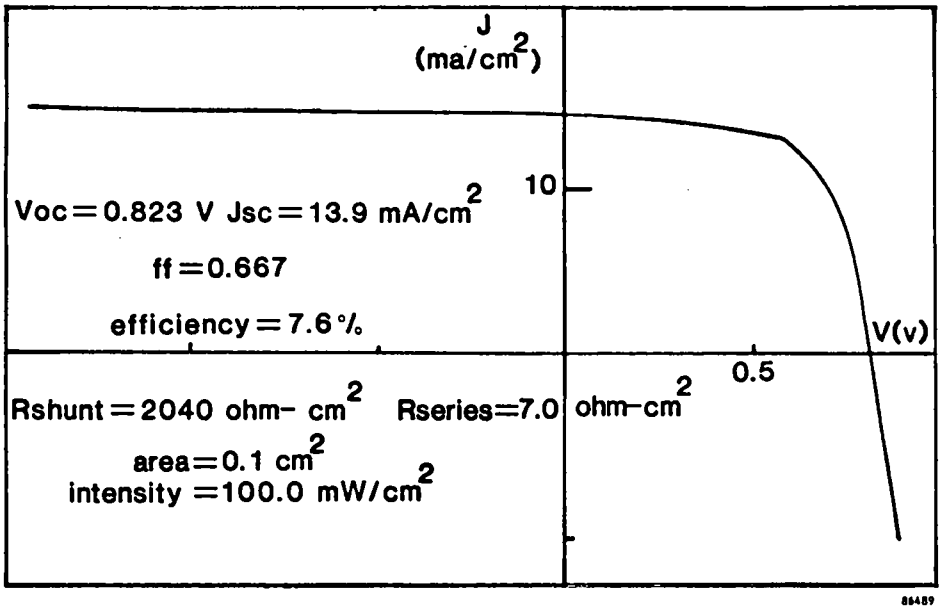

FIGURE 5-3. I-V CHARACTERISTICS OF a-Si:H CELL 20286-C3 WITH A p-i-n-p CONFIGURATION.

5.2 MODELLING

A program has been developed which calculates I-V curves of series-connected tandem cells. The program steps through 101 values of current, solving for the junction voltages of the top and bottom cells. Junction voltages are converted to cell voltages for the top, bottom, and tandem cell. Power is then calculated. After generating the I-V curve, the program goes back to home in on the maximum power point of each cell, and V_{oc}, FF, I_{max} and V_{max} are then calculated.

The model assumes two cells in series, each with a double exponential diode characteristic, series resistance and short resistance. Specifically, the model works with the following set of equations:

1) $V = V_1 + V_2 + I(R_{S1} + R_{S2})$

2) $I = I_1(V_1) - I_{L1} + V_1/R_{SH1} = I_2(V_2) - I_{L2} + V_2/R_{SH2}$

3) $I_1(V_1) = I_{1-1}(\exp [qV_1/n_{11}kT] - 1) + I_{102} (\exp [qV_1/n_{12}kT] - 1)$

4) $I_2(V_2 = I_{201} (\exp [qV_2/n_{21}kT] - 1) + I_{202} (\exp [qV_2/n_{22}kT] - 1)$

Details are given in Appendix A.

The reason for developing the program is to provide guidance in the on-going research and development efforts for tandem cells. A model based on the optical constants of the various materials incorporated in single and tandem devices is also being developed to assist in the research efforts.

5.3 TANDEM CELL STABILITY UNDER PROLONGED ILLUMINATION

Stability tests were carried out on both single-junction and tandem solar cells. The accelerated stress-test routine is as follows:

1. Test I-V characteristics and QE.
2. Light stressing under 200 mW/cm^2 illumination from an ELH lamp with continuous monitoring of V_{OC}.
3. Remove cell from accelerated stress facility and retest I-V and QE.
4. Continue accelerated stress and retest sequence.

Typical results of the exosure of several cells to the above routine are presented in Appendix B.

REFERENCES

1. R. Gordon et al., Final Report to SERI, Subcontract No. XS-0-9318-2 (October 1984).

2. V.L. Dalal et al., Annual Report to SERI for Phase II of Subcontract ZB-04-03055-1 (February 1986).

3. C.A. Megerie et al., Proc. 17th IEEE PV Specialists Conference, p. 212 (1984).

4. A. Catalano et al., Proc. 16th IEEE PV Specialists Conference, p. 1421 (1982).

5. F. Evangelista et al., Proc. Mat. Res. Soc. Meeting, San Francisco, p. 95 (1985).

6. T. Tiedje et al., J. Non-Crystalline Solids, Vol. 77-78, p. 1031 (1985)

7. K. Mitchell et al., Proc. 18th IEEE PV Specialists Conference, p. 894 (1985).

APPENDIX A

PROGRAM TO CALCULATE I-V CURVES OF SERIES-CONNECTED TANDEM CELLS

The following describes a Fortran program which calculates I-V curves of series-connected tandem cells.

MODEL: Series connection of two cells, each with a double exponential diode characteristic, series resistance, and shunt resistance.

1) $V = V_1 + V_2 + I(R_{S1} + R_{S2})$

2) $I = I_1(V_1) - I_{ph1} + V_1/R_{SH1} = I_2(V_2) - I_{ph2} + V_2/R_{SH2}$

3) $I_1(V_1) = I_{101}(\exp[qV_1/n_{11}kT] - 1) + I_{102}(\exp[qV_1/n_{12}kT] - 1)$

4) $I_2(V_2) = I_{201}(\exp[qV_2/n_{21}kT] - 1) + I_{202}(\exp[qV_2/n_{22}kT] - 1)$

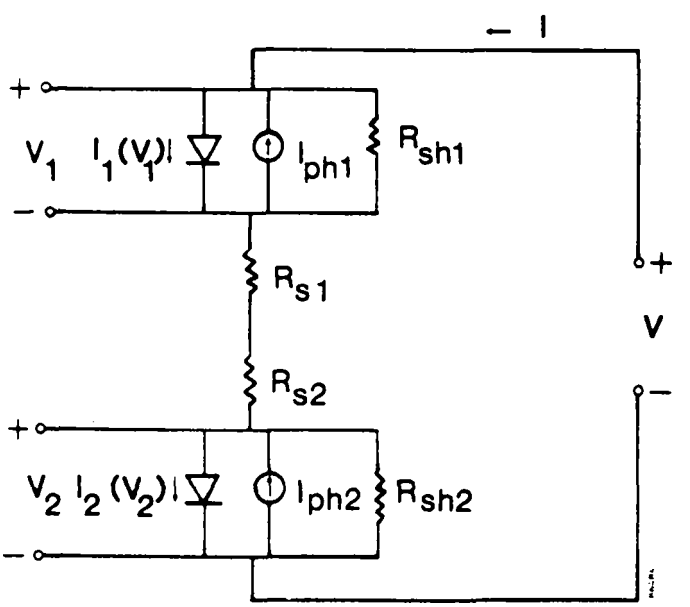

COMPUTER PROGRAMS

TANDEM.EXE

Lists out on printer:

- Input cell parameters
- Top cell efficiency results (independent operation)
- Bottom cell efficiency results (ind. operation)
- Tandem cell efficiency results

TAND2.EXE

Same output to printer, plus:

- creates data file of I,V (tandem), V(top), V(bottom) (101 points).

ALGORITHM

The program steps through 101 values of current, solving for the junction voltages of the top and bottom cells (Newton's method to solve [2] and [3]). Junction voltages are converted to cell voltages for the top, bottom, and tandem cells. Power is then calculated, and the maximum power for each cell is stored.

After generating the I-V curve, the program goes back to home in on the maximum power point of each cell. V_{oc}, FF, I_m, and V_m are then calculated.

The program prints out all of the inout values and the relevant calculated values for each cell: P_m, V_m, I_m, V_{oc}, I_{sc}, FF. If TAND2 is being used, a data file is created for the I-V data.

IMPLEMENTATION

The programs are run as executable files on an IBM PC. They were written for a machine with the 8087 math coprocessor, and will not work without it. A hard disk is not necessary, but is desirable if lots of data files are being created. The programs were written in Fortran and compiled with the Microsoft Fortran compiler. If changes need to be made, the programs must be recompiled.

GRAPHING THE I-V CURVES

It's usually easier to see what's going on with I-V curves than tables of numbers. On the diskette is another program in BASIC called "GRAPH" that will plot out the I-V curves (or any data, for that matter). To use it:

1. Run TAND2 to create data files of the I-V curves
2. GRAPHICS (to allow printing of the graphics screen)
3. BASICA
4. Load "GRAPH"
5. Run

GRAPH walks you through the process of (1) defining axes (2) loading data and (3) plotting the curve. The graph appears on the CRT screen, where it can be copied to the printer by PrtSc. BASICA version A2.10 was used, and DOS version 3.1. Text can be added to or deleted from the screen by positioning the cursor and typing. Don't use the carriage return or backspace keys, though. Typical output and a sample terminal session are appended.

```
************************************************************************
*                                                                      *
      PROGRAM TANDEM
*                                                                      *
********************  PROGRAM  IDENTIFICATION  ***********************
*                                                                      *
*     TANDEM CELL I-V CHARACTERISTICS CALCULATION                      *
*     WRITTEN 02-10-86 BY S. TOBIN                                     *
*     LAST REVISION 02-12-86 BY S. TOBIN                               *
*                                                                      *
********************  PROGRAM  DESCRIPTION  **************************
*                                                                      *
*     THIS PROGRAM CALCULATES THE ILLUMINATED I-V CHARACTERISTICS      *
*     OF A SERIES-CONNECTED TANDEM CELL, USING DOUBLE-EXPONENTIAL      *
*     MODELS OF THE TWO COMPONENT CELLS WITH SERIES AND SHUNT          *
*     RESISTANCES INCLUDED.  THE I-V CHARACTERISTICS OF THE            *
*     COMPONENT CELLS ARE ALSO CALCULATED, FOR INDEPENDENT             *
*     OPERATION.                                                       *
*                                                                      *
************************************************************************
*                                                                      *
      INTEGER J,K,REP,JMT,JM1,JM2,VNEGT,VNEG1,VNEG2,JENDT,JEND1,JEND2
      INTEGER ERR,JM11
      REAL I101,N11,I102,N12,RS1,RSH1,I201,N21,I202,N22,RS2,RSH2
      REAL IPH1,IPH2,IMAX,KTQ,STEP,I(150),VT(150),V1(150),V2(150)
      REAL PT(150),P1(150),P2(150),VFT,VF1,VF2,RST,ISCT,ISC1,ISC2
      REAL PMT,PM1,PM2,VOCT,VOC1,VOC2,FFT,FF1,FF2,IMT,IM1,IM2
      REAL VMT,VM1,VM2,LO,HI,I1(150),I2(150),IT(150)
*                                                                      *
*****    Input parameters from keyboard                               *
*                                                                      *
   80 WRITE(*,*)' Enter for top cell: '
      WRITE(*,*)'   Io1, n1, Io2, n2, Rseries, Rshunt (amp, ohm)'
      READ(*,*)I101,N11,I102,N12,RS1,RSH1
      WRITE(*,*)' Enter for bottom cell: '
      WRITE(*,*)'   Io1, n1, Io2, n2, Rseries, Rshunt (amp, ohm)'
      READ(*,*)I201,N21,I202,N22,RS2,RSH2
  100 WRITE(*,*)' Enter photocurrents for top and bottom cells : (mA)'
      READ(*,*)IPH1,IPH2
      IPH1=IPH1*.001
      IPH2=IPH2*.001
      OPEN(3,FILE='PRN',STATUS='OLD')
*                                                                      *
*****    Calculate I-V curve (100 points evenly spaced in current)    *
         *
*                                                                      *
      ERR=0
      KTQ=.02595
      PMT=0
      PM1=0
      PM2=0
      VNEGT=0
      VNEG1=0
      VNEG2=0
      IMAX=MAX(IPH1,IPH2)
      STEP=IMAX/100
      DO 500 J=1,101
         I(J)=-(J-1)*STEP
*                                                                      *
*****       Solve for junction voltage of top and bottom cell         *
 *
```

```
*                                                                       *
          CALL VJUNCT(N11,I101,N12,I102,RSH1,IPH1,VF1,J,I,KTQ,ERR)
             IF(ERR.EQ.1) GOTO 1500
          CALL VJUNCT(N21,I201,N22,I202,RSH2,IPH2,VF2,J,I,KTQ,ERR)
             IF(ERR.EQ.1) GOTO 1500
*                                                                       *
*****        Construct I-V curves of tandem, top and bottom cells      *
*                                                                       *
          VFT=VF1+VF2
          RST=RS1+RS2
          CALL POW(VFT,RST,ISCT,VT,PT,PMT,JMT,VNEGT,JENDT,I,J,ERR)
             IF(ERR.EQ.1) GOTO 1500
          CALL POW(VF1,RS1,ISC1,V1,P1,PM1,JM1,VNEG1,JEND1,I,J,ERR)
             IF(ERR.EQ.1) GOTO 1500
          CALL POW(VF2,RS2,ISC2,V2,P2,PM2,JM2,VNEG2,JEND2,I,J,ERR)
             IF(ERR.EQ.1) GOTO 1500
  500     CONTINUE
*                                                                       *
*****    Home in on maximum power point for each cell                   *
*                                                                       *
*         Top Cell
*
          LO=I(JM1-1)
          HI=I(JM1+1)
          STEP=(HI-LO)/20
        DO 600 J=110,130
          I1(J)=LO+(J-110)*STEP
          CALL VJUNCT(N11,I101,N12,I102,RSH1,IPH1,VF1,J,I1,KTQ,ERR)
             IF(ERR.EQ.1) GOTO 1500
          CALL POW(VF1,RS1,ISC1,V1,P1,PM1,JM1,VNEG1,JEND1,I1,J,ERR)
             IF(ERR.EQ.1) GOTO 1500
  600     CONTINUE
*
*        Bottom Cell
*
          LO=I(JM2-1)
          HI=I(JM2+1)
          STEP=(HI-LO)/20
        DO 700 J=110,130
          I2(J)=LO+(J-110)*STEP
          CALL VJUNCT(N21,I201,N22,I202,RSH2,IPH2,VF2,J,I2,KTQ,ERR)
             IF(ERR.EQ.1) GOTO 1500
          CALL POW(VF2,RS2,ISC2,V2,P2,PM2,JM2,VNEG2,JEND2,I2,J,ERR)
             IF(ERR.EQ.1) GOTO 1500
  700     CONTINUE
*
*        Tandem Cell
*
          LO=I(JMT-1)
          HI=I(JMT+1)
          STEP=(HI-LO)/20
        DO 800 J=110,130
          IT(J)=LO+(J-110)*STEP
          CALL VJUNCT(N11,I101,N12,I102,RSH1,IPH1,VF1,J,IT,KTQ,ERR)
             IF(ERR.EQ.1) GOTO 1500
          CALL VJUNCT(N21,I201,N22,I202,RSH2,IPH2,VF2,J,IT,KTQ,ERR)
             IF(ERR.EQ.1) GOTO 1500
          VFT=VF1+VF2
          RST=RS1+RS2
          CALL POW(VFT,RST,ISCT,VT,PT,PMT,JMT,VNEGT,JENDT,IT,J,ERR)
             IF(ERR.EQ.1) GOTO 1500
  800     CONTINUE
*                                                                       *
```

```
*****   Calculate Voc, FF, Im, and Vm for each cell                    *
*                                                                      *
      CALL EFF(VOCT,VT,FFT,PMT,ISCT,IMT,VMT,JMT,IT,ERR)
         IF(ERR.EQ.1) GOTO 1500
      CALL EFF(VOC1,V1,FF1,PM1,ISC1,IM1,VM1,JM1,I1,ERR)
         IF(ERR.EQ.1) GOTO 1500
      CALL EFF(VOC2,V2,FF2,PM2,ISC2,IM2,VM2,JM2,I2,ERR)
         IF(ERR.EQ.1) GOTO 1500
*                                                                      *
*****   List input parameters and results on printer                   *
*                                                                      *
      WRITE(3,*)'          TOP CELL                    BOTTOM CELL '
      WRITE(3,1000)I101,I201
      WRITE(3,1001)N11,N21
      WRITE(3,1002)I102,I202
      WRITE(3,1003)N12,N22
      WRITE(3,1004)RS1,RS2
      WRITE(3,1005)RSH1,RSH2
      WRITE(3,1006)IPH1*1000,IPH2*1000
      WRITE(3,1050)PM1*1000,PM2*1000
      WRITE(3,1051)VM1,VM2
      WRITE(3,1052)IM1*1000,IM2*1000
      WRITE(3,1053)VOC1,VOC2
      WRITE(3,1054)ISC1*1000,ISC2*1000
      WRITE(3,1055)FF1,FF2
      WRITE(3,1100)PMT*1000
      WRITE(*,1100)PMT*1000
      WRITE(3,1101)VMT
      WRITE(*,1101)VMT
      WRITE(3,1102)IMT*1000
      WRITE(*,1102)IMT*1000
      WRITE(3,1103)VOCT
      WRITE(*,1103)VOCT
      WRITE(3,1104)ISCT*1000
      WRITE(*,1104)ISCT*1000
      WRITE(3,1105)FFT
      WRITE(*,1105)FFT
 1000 FORMAT(/,5X,'Io1 = ',E11.4,' A',6X,'Io1 = ',E11.4,' A')
 1001 FORMAT(6X,'n1 = ',F6.3,14X,'n1 = ',F6.3)
 1002 FORMAT(5X,'Io2 = ',E11.4,' A',6X,'Io2 = ',E11.4,' A')
 1003 FORMAT(6X,'n2 = ',F6.3,14X,'n2 = ',F6.3)
 1004 FORMAT(6X,'Rs = ',F8.5,' ohm',8X,'Rs = ',F8.5,' ohm')
 1005 FORMAT(5X,'Rsh = ',E11.4,' ohm',4X,'Rsh = ',E11.4,' ohm')
 1006 FORMAT(5X,'Iph = ',F8.3,' mA',8X,'Iph = ',F8.3,' mA')
 1050 FORMAT(/,6X,'Pm = ',F8.3,' mW',9X,'Pm = ',F8.3,' mW')
 1051 FORMAT(6X,'Vm = ',F6.4,' V',12X,'Vm = ',F6.4,' V')
 1052 FORMAT(6X,'Im = ',F8.3,' mA',9X,'Im = ',F8.3,' mA')
 1053 FORMAT(5X,'Voc = ',F6.4,' V',11X,'Voc = ',F6.4,' V')
 1054 FORMAT(5X,'Isc = ',F8.3,' mA',8X,'Isc = ',F8.3,' mA')
 1055 FORMAT(6X,'FF = ',F6.4,14X,'FF = ',F6.4)
 1100 FORMAT(///,20X,'TANDEM CELL',//,16X,'Pm = ',F8.3,' mW')
 1101 FORMAT(16X,'Vm = ',F6.4,' V')
 1102 FORMAT(16X,'Im = ',F8.3,' mA')
 1103 FORMAT(15X,'Voc = ',F6.4,' V')
 1104 FORMAT(15X,'Isc = ',F8.3,' mA')
 1105 FORMAT(16X,'FF = ',F6.4,//)
*                                                                      *
*****   Repeat the calculation with different parameters or quit       *
*                                                                      *
      CLOSE(3)
      WRITE(*,*)' Choose from :    1  Change photocurrents & repeat '
      WRITE(*,*)'                  2  Change all parameters & repeat '
      WRITE(*,*)'                  3  End '
```

```
      READ(*,*)REP
      IF(REP.EQ.1) GOTO 100
      IF(REP.EQ.2) GOTO 80
 1500 CLOSE(3)
      END
*************************************************************************
*                                                                       *
      SUBROUTINE VJUNCT(N1,IO1,N2,IO2,RSH,IPH,VF,J,I,KTQ,ERR)
*                                                                       *
********************  SUBROUTINE DESCRIPTION  ************************
*                                                                       *
*     THIS SUBROUTINE CALCULATES THE JUNCTION VOLTAGE OF A              *
*     SOLAR CELL AT A GIVEN CURRENT I(J).                               *
*                                                                       *
*************************************************************************
*                                                                       *
      INTEGER J,K,ERR
      REAL N1,IO1,N2,IO2,RSH,IPH,VF,VJ(10),I(150),KTQ,VN,NUM
      REAL F,FDER,CORR,DEC,ID
      ID=IPH+I(J)
      IF(ID.LE.0) THEN
         VJ(1)=ID*RSH
      ELSE
         IF(IO1.EQ.0) THEN
            WRITE(*,*)' Divide by zero in line 168 (IO1)  J=',J
            ERR=1
            RETURN
         ENDIF
  168    VJ(1)=N1*KTQ*LOG(ID/IO1)
      ENDIF
      VN=VJ(1)
      DO 300 K=2,10
         IF(KTQ.EQ.0) THEN
            WRITE(*,*)' Divide by zero in line 177 (KTQ)  J=',J
            ERR=1
            RETURN
         ENDIF
  177    NUM=VN/KTQ
         IF((N1.EQ.0).OR.(N2.EQ.0).OR.(RSH.EQ.0)) THEN
            WRITE(*,*)' Divide by zero in line 187 (N1,N2 or RSH) J=',J
            ERR=1
            RETURN
         ENDIF
         IF(NUM.LT.-30) THEN
            F=-IO1-IO2-ID+VN/RSH
            FDER=1/RSH
         ELSE
  187       F=IO1*(EXP(NUM/N1)-1)+IO2*(EXP(NUM/N2)-1)-ID+VN/RSH
            FDER=IO1/N1/KTQ*EXP(NUM/N1)+IO2/N2/KTQ*EXP(NUM/N2)
            FDER=FDER+1/RSH
         ENDIF
         IF(FDER.EQ.0) THEN
            WRITE(*,*)' Divide by zero in line 196 (FDER)  J=',J
            ERR=1
            RETURN
         ENDIF
  196    CORR=F/FDER
         VJ(K)=VJ(K-1)-CORR
         DEC=ABS(CORR)
         IF(DEC.LT.0.0001) GOTO 350
  300    VN=VJ(K)
      WRITE(*,*)' Too many iterations for V at I= ',I(J)
  350 VF=VJ(K)
```

```
      RETURN
      END
*****************************************************************************
*                                                                           *
      SUBROUTINE POW(VF,RS,ISC,V,P,PM,JM,VNEG,JEND,I,J,ERR)
*                                                                           *
*********************  SUBROUTINE DESCRIPTION  **************************
*                                                                           *
*     THIS SUBROUTINE CALCULATES CELL VOLTAGE AND POWER FOR A               *
*     GIVEN CURRENT AND PICKS OUT Isc AND Pmax.                             *
*                                                                           *
*****************************************************************************
*                                                                           *
      INTEGER J,JEND,VNEG,JM,ERR
      REAL V(150),VF,I(150),RS,ISC,P(150),PM
      V(J)=VF+I(J)*RS
      IF(V(J).LT.0) THEN
         VNEG=VNEG+1
         IF(VNEG.EQ.1) THEN
            JEND=J
            IF(V(J-1).EQ.V(J)) THEN
               WRITE(*,*) ' Divide by zero in line 228  J=',J
               ERR=1
               RETURN
            ENDIF
  228       ISC=-(I(J-1)+V(J-1)*(I(J)-I(J-1))/(V(J-1)-V(J)))
         ENDIF
      ENDIF
      P(J)=-I(J)*V(J)
      IF(P(J).GE.PM) THEN
         JM=J
         PM=P(J)
      ENDIF
      RETURN
      END
*****************************************************************************
*                                                                           *
      SUBROUTINE EFF(VOC,V,FF,PM,ISC,IM,VM,JM,I,ERR)
*                                                                           *
*********************  SUBROUTINE DESCRIPTION  **************************
*                                                                           *
*     THIS SUBROUTINE CALCULATES Voc, FF, Im, AND Vm                        *
*                                                                           *
*****************************************************************************
*                                                                           *
      INTEGER JM,ERR
      REAL VOC,V(150),FF,PM,ISC,IM,VM,I(150)
      VOC=V(1)
      IF((VOC.EQ.0).OR.(ISC.EQ.0)) THEN
         WRITE(*,*)' Divide by zero in line 216 (VOC or ISC)'
         ERR=1
         RETURN
      ENDIF
  216 FF=PM/VOC/ISC
      IM=-I(JM)
      VM=V(JM)
      RETURN
      END
```

SAMPLE TERMINAL SESSION

(User responses underlined)

A)tand2
 Enter for top cell:
   Io1, n1, Io2, n2, Rseries, Rshunt (amp, ohm)
1e-22,1.1e-13,2,1,10000
 Enter for bottom cell:
   Io1, n1, Io2, n2, Rseries, Rshunt (amp, ohm)
1e-12,1.1e-9,2,1,10000
 Enter photocurrents for top and bottom cells : (mA)
20,20
 Enter name of data file for output :
plotiv.dat

(See next page for Printer Output)

TANDEM CELL

Pm = 30.847 mW
Vm = 1.6050 V
Im = 19.220 mA
Voc = 1.8263 V
Isc = 19.995 mA
FF = .8448

Choose from : 1 Change photocurrents & repeat
2 Change all parameters & repeat
3 End

3

A)graphics

A)basica

The IBM Personal Computer Basic
Version A2.10 Copyright IBM Corp. 1981, 1982, 1983
60891 Bytes free

Ok
LOAD"graph
Ok
run

Choose between : 0 to escape
1 to input axes
2 to input data points
3 to plot : 1

SAMPLE PRINTER OUTPUT FROM "TANDEM" OR "TAND2"

TOP CELL		BOTTOM CELL	
Io1 =	.1000E-21 A	Io1 =	.1000E-11 A
n1 =	1.000	n1 =	1.000
Io2 =	.1000E-12 A	Io2 =	.1000E-08 A
n2 =	2.000	n2 =	2.000
Rs =	1.00000 ohm	Rs =	1.00000 ohm
Rsh =	.1000E+05 ohm	Rsh =	.1000E+05 ohm
Iph =	20.000 mA	Iph =	20.000 mA
Pm =	21.069 mW	Pm =	9.814 mW
Vm =	1.0905 V	Vm =	.5182 V
Im =	19.320 mA	Im =	18.940 mA
Voc =	1.2110 V	Voc =	.6152 V
Isc =	19.996 mA	Isc =	19.992 mA
FF =	.8701	FF =	.7979

TANDEM CELL

Pm =	30.847 mW
Vm =	1.6050 V
Im =	19.220 mA
Voc =	1.8263 V
Isc =	19.995 mA
FF =	.8448

```
x axis: log or lin  lin
y axis: log or lin  lin
input xmin,xmax,xint:  0,2,.2
input ymin,ymax,yint:  0,.024,.002
x axis label:   Voltage (V)
y axis label:   Current (A)


   Choose between :  0  to escape
                     1  to input axes
                     2  to input data points
                     3  to plot                    : 2


input number of curves to be graphed: 3


For curve number  1
   Choose between :  1  for file data
                     2  for data input from keyboard
                     3  for previous data          : 1
input name of data file:  plotiv.dat
positions of x and y variables in the file :  2,1
connect data points? (y/n)  y
draw symbols at data points? (y,n)  n
Modify or file input data?  (y,n) n


For curve number  2
   Choose between :  1  for file data
                     2  for data input from keyboard
                     3  for previous data          : 1
input name of data file:  plotiv.dat
positions of x and y variables in the file :  3,1
connect data points? (y/n)  y
draw symbols at data points? (y,n)  n
Modify or file input data?  (y,n) n


For curve number  3
   Choose between :  1  for file data
                     2  for data input from keyboard
                     3  for previous data          : 1
input name of data file:  plotiv.dat
positions of x and y variables in the file :  4,1
connect data points? (y/n)  y
draw symbols at data points? (y,n)  n
Modify or file input data?  (y,n) n


   Choose between :  0  to escape
                     1  to input axes
                     2  to input data points
                     3  to plot                    : 3
```

(See next page for Printer Output)

SAMPLE PRINTER OUTPUT FROM "GRAPH"

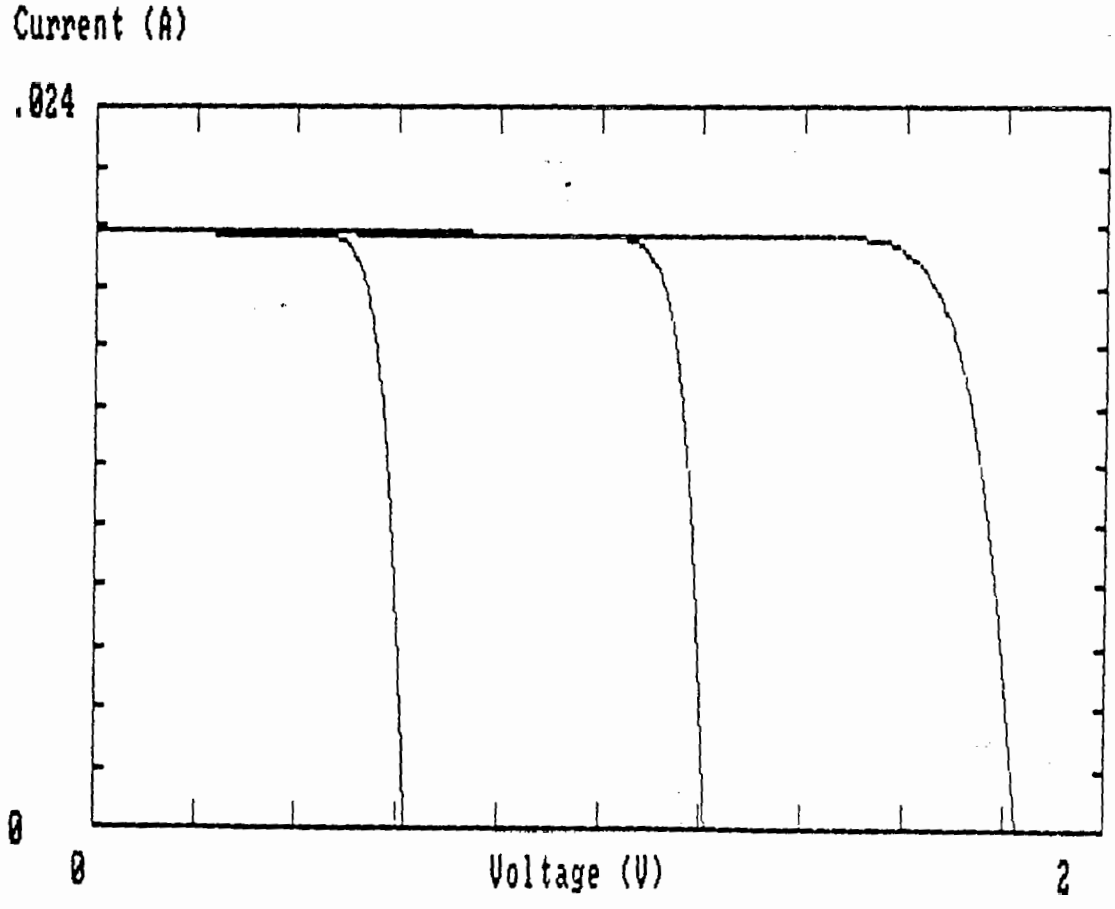

```
Choose between :  0  to escape
                  1  to input axes
                  2  to input data points
                  3  to plot                    : 0
```

```
Ok
system

A>
```

TOP CELL		BOTTOM CELL	
Io1 =	.1000E-21 A	Io1 =	.1000E-10 A
n1 =	1.000	n1 =	1.000
Io2 =	.1000E-12 A	Io2 =	.1000E-07 A
n2 =	2.000	n2 =	2.000
Rs =	.10000 ohm	Rs =	10.00000 ohm
Rsh =	.1000E+05 ohm	Rsh =	.1000E+04 ohm
Iph =	20.000 mA	Iph =	20.000 mA
Pm =	21.406 mW	Pm =	5.614 mW
Vm =	1.1068 V	Vm =	.3338 V
Im =	19.340 mA	Im =	16.820 mA
Voc =	1.2110 V	Voc =	.5544 V
Isc =	20.000 mA	Isc =	19.802 mA
FF =	.8838	FF =	.5114

TANDEM CELL

Pm =	26.445 mW
Vm =	1.4052 V
Im =	18.820 mA
Voc =	1.7655 V
Isc =	19.968 mA
FF =	.7502

Sample Output:

Matched (this page) and Mismatched (next page) Cells

Currents Matched at 20 mA

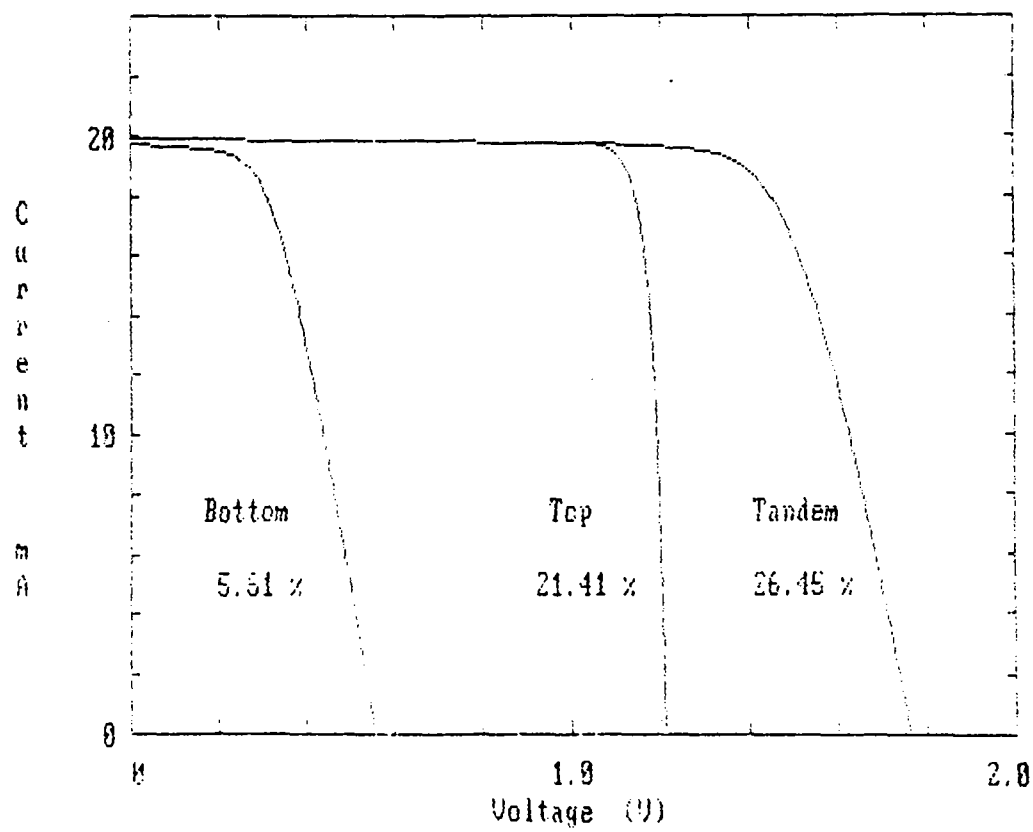

Top Cell 22 mA, Bottom Cell 18 mA

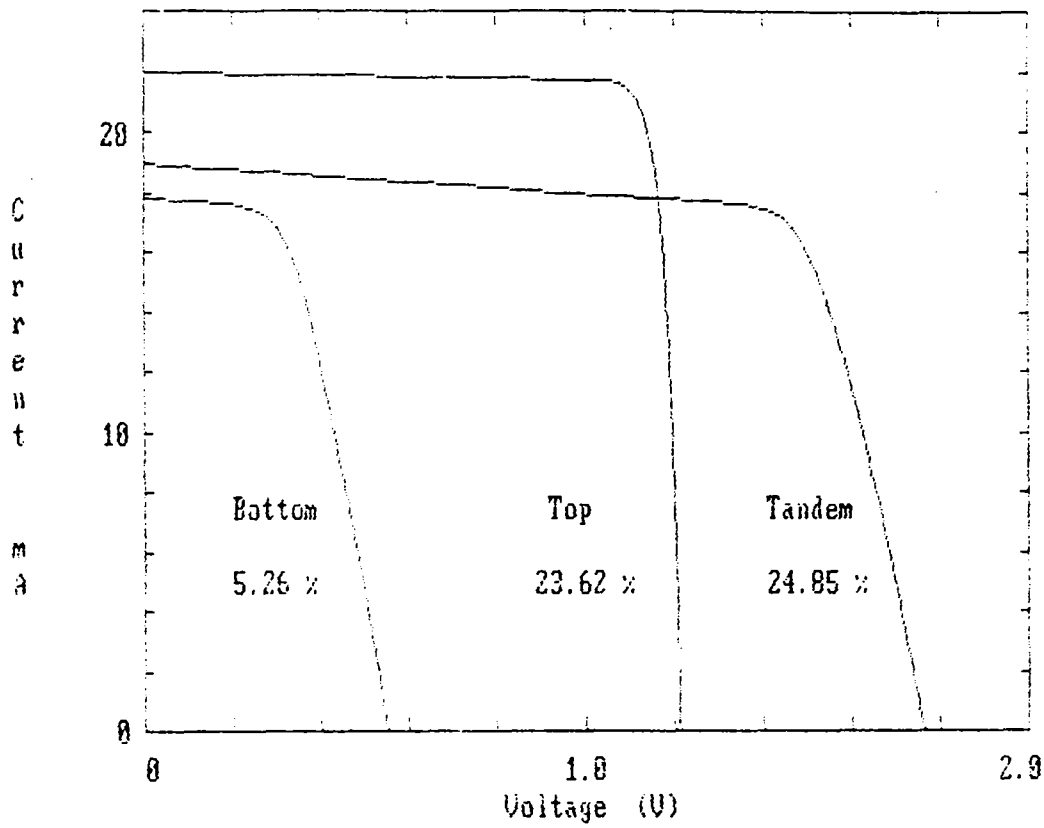

Top Cell 18 mA, Bottom Cell 22 mA

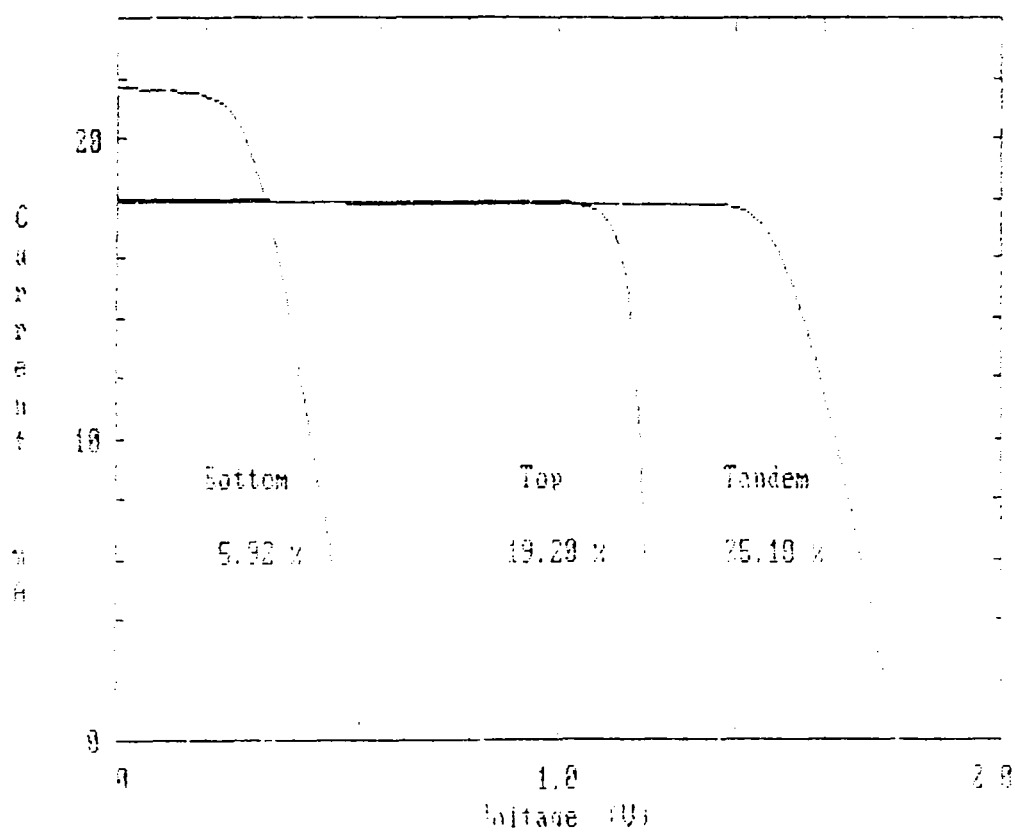

APPENDIX B
DEVICE STABILITY

1.0 INTRODUCTION

It is well known that a-Si:H cells suffer a degradation in efficiency upon exposure to light.[1] This effect, known as the Stabler-Wronski effect, is due to additional defect states being introduced in the mid-gap region upon light exposure.[2] The question that a device designer wants to answer is: what is the impact of additional states on device parameters.[2] In this Appendix, we shall show that the creation of mid-gap states can have significant impact on both electron and hole properties, and that the changes in these properties lead to very different impacts on single-junction and tandem-junction cells.

2.0 IMPACT OF STABLER-WRONSKI EFFECT ON ELECTRONS AND HOLES

The creation of mid-gap defects upon light exposure has several impacts on electronic properties of the material.

(i) Mid-gap defects create additional recombination centers.

(ii) The creation of additional defects in the middle of the gap tends to bring Fermi level down from its initial position of ~0.7-0.8 eV below the conduction band. Thus, dark conductivity decreases.

(iii) The movement of Fermi level downwards has a particularly severe impact on electron lifetime (τ_e), since now more mid-gap states are empty (see Figure B-1) and so τ_e decreases. Thus, electron ($\mu\tau$) product decreases, and hence, photoconductivity decreases rather rapidly.

(iv) The creation of additional mid-gap defects decreases hole lifetime, since there are now more recombination centers than before.

Thus, both electron and hole ($\mu\tau$) products decreases, with the electron ($\mu\tau$) decreasing much more (because of the movement of the Fermi level) than the hole ($\mu\tau$) product.

3.0 IMPACT OF DECREASE IN ELECTRON AND HOLE ($\mu\tau$) PRODUCTS ON DEVICE PROPERTIES OF SINGLE JUNCTION DEVICES

A. Decrease in Electron $\mu\tau$

The decrease in electron ($\mu\tau$) can have two consequences. First, the back-diffusion of electrons toward the p^+ layer relative to drift away from the p^+ layer increases. This can be seen from the following relationship. The drift range away from the p-i interface is given by $\mu\tau E$, where E is the field. The diffusion length towards the p-layer is given by:

$$L = \sqrt{(\mu\tau kT/q)}$$

The ratio of diffusion to drift is given by:

$$1/E\sqrt{kT/(q \cdot \mu\tau)}$$

Thus, as $\mu\tau$ decreases, the ratio of diffusion to drift increases. Therefore, we expect a decrease in quantum efficiency (QE) in the 400-500 nm region as electron $\mu\tau$ decreases.

Next, as electron $\mu\tau$ decreases in the bulk of the i-layer, the photoconductivity decreases. Thus, the series resistance increases. Therefore, fill factor will decrease.

Thus, decrease in electron $\mu\tau$ will cause both a decrease in collection efficiency and a decrease in fill factor due to increasing series resistance.

B. Decrease in Hole $\mu\tau$

As hole $\mu\tau$ product decreases, the diffusion length and range ($\mu\tau E$) both decrease. Thus, one expects a decrease in collection efficiency of holes, particularly under forward bias, and a resultant decrease in fill factor. The decrease in collection efficiency of holes should be readily evident by looking at QE at 700 nm.

C. Experimental Results

In Figure B-2, we show the I(V) curve for an a-Si:H single junction cell before light degradation. The series resistance is composed of two parts - contact (SnO_2) and intrinsic material. The contact resistance is small, ≤ 2 ohms/cm^2. The QE curve for the device is shown in Figure B-3.

In Figure B-4, we plot the device resistance, fill factor, voltage, and current as a function of the time under light illumination of 200 mW/cm^2 of ELH lamp. Quite clearly, the major degradation is in fill factor, attendant with a very large increase in series resistance. The series resistance increases from 5.8 ohms-cm^2 before light soaking to 13.5 ohms-cm^2 after 125 hours. Correspondingly, the fill factor drops from 0.67 to 0.51. The current changes from 13.0 mA/cm^2 to 12.0 mA/cm^2, and the voltage from 737 mV to 723 mV.

Now let us see if the measured decrease in fill factor can be explained by the increase in series resistance. To a first approximation, the decrease in fill factor due to increased series resistance is given by:

$$I \cdot [(R_{s2})-(R_{s1})] V_{max}$$

where R_{s2} is the resistance after degradation, and R_{s1} is the resistance before degradation and V_{max} is the voltage at maximum power.

$$\Delta FF = \frac{13\,(13.5-5.8)}{600} = 0.17.$$

The observed decrease is 0.16. Quite obviously, then, most of the decrease in fill factor is directly related to an increase in series resistance, or a decrease in electron $\mu\tau$ product.

Now let us see how QE of the device changes upon light soaking. An effective way to see changes in QE is to plot the QE ratio, QE(-1v)/QE(0v), vs. wavelength. We plot this ratio in Figure B-5 before and after light soaking. We see that the ratio has gone up at 400 nm, and at 700 nm, the former being an indication of collection problems of electrons, and the

latter, of holes. Thus, both electron and hole ($\mu\tau$) products have decreased upon light soaking, as expected from our discussion in Section 2.0.

4.0 IMPACT OF STABLER-WRONSKI EFFECT ON PROPERTIES OF a-Si/a-Si 2-JUNCTION TANDEM JUNCTION CELLS

A. Decrease in Electron $\mu\tau$

A decrease in electron $\mu\tau$ would impact the current in the first cell most, since it is the cell in which the electron back diffusion, is likely to be most prominent. (All the strongly absorbed light, which leads to electron back diffusion, is absorbed in the first cell). Thus, we expect a decrease in current of the first cell. The effect of increasing resistance would not be strongly felt in the first cell, since its i-layer is thin. ($\sim$ 100 nm).

In contrast, in the second cell, decreasing electron $\mu\tau$ would increase the series resistance, leading to a loss in fill factor.

B. Decrease in Hole ($\mu\tau$) Product

A decrease in hole ($\mu\tau$) product would lead to a loss in collection efficiency of the second cell, leading to a slight decrease in current.

C. Experimental Results

We show the experimental results for a two-terminal a-Si/a-Si tandem cell in Figure B-6. There, we plot J_{SC}, FF and V_{OC} vs. illumination time under continuous illumination of 200 mW/cm^2 from an ELH lamp. The current decreases by 6%, the voltage by 2%, and the fill factor by 13%.

The decrease in current is consistent with what can be expected on the basis of loss of QE in the first cell. In our single cell work, we saw that the current decreased by about 1.0 mA/cm^2, and the QE loss was both in the blue and red regions of the spectrum. Thus, in a tandem cell, we expect the loss in current to be 1.0 mA cm^2, which is what we observe.

The remarkable observation about tandem cells is that the fill factor decreases is much less than in a single cell. This fact can be explained by saying that the impact of increase is series resistance is much less in a tandem cell, since the percentage loss due to series resistance is reduced by a factor of four in a two-junction tandem cell compared to a single cell.[4] (The voltage in a tandem cell is approximately twice, and current, approximately half, that in a single cell. Hence IR/V is 1/4 that of a single cell.) Thus, an increase in R series from 24 ohms/cm^2 to 47 ohms/cm^2 after 275 hours of 200 mW/cm^2 should decrease fill factor by 0.09. The actual decrease is also 0.09, as opposed to 0.16 in the single junction case.

The other remarkable fact to notice in tandem junction cells is that the degradation is essentially stabilized within about 50 hours.

5.0 CONCLUSIONS

From our study of the degradation of a-Si:H solar cells, we conclude that both electrons and holes play a part in degradation, and that the increase in series resistance due to a

decrease in electron ($\mu\tau$) is a primary contributor to the loss in fill factor. Our results cannot be explained by the simple theory of collection length of Crandall,[5,6] which assumes that the collection of carriers is controlled by the sum of electron and hole. Crandall's theory is clearly wrong, because what is says is that if we can increase the electron $\mu\tau$ but decrease hole $\mu\tau$, as can be done with a few ppm PH_3 doping, the cell efficiency will improve. This is quite contrary to the experimental results, where a few ppm PH_3 doping reduces the efficiency significantly. To analyze stability, one has to look individually at electron and hole properties, and not at the sum.

REFERENCES

1. See for example, Solar Cells, Vol. 9 (1983). (Issue on Stability)

2. R. Street, Appl. Phys. Lett. 42, 507 (1983).

3. V. L. Dalal, J. Booker, M. Leonard, A. Vaseashta, S. Hegedus, Proc. of 19th IEEE Photovolt. Conf. (Las Vegas, 1985).

4. V. L. Dalal, Proc. of 18the IEEE Photovolt. Conf. (Orlando, FL 1984) p. 86.

5. R. Crandall, Solar Cells (1983).

6. Z. E. Smith and S. Wagner, Appl. Phys. Lett., 11 1078 (1985).

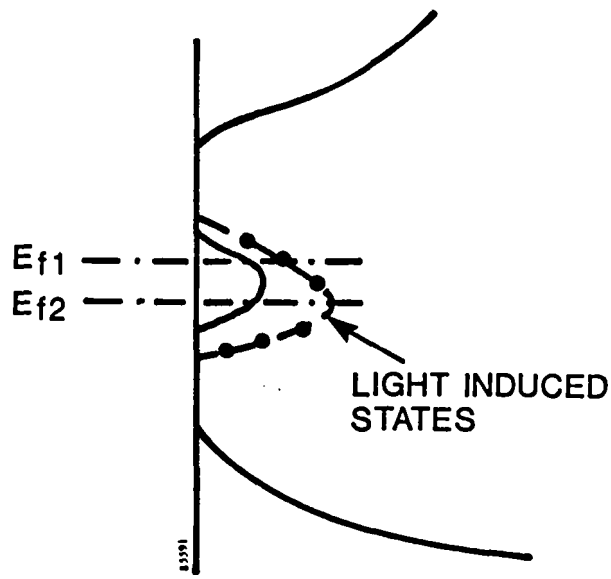

FIGURE B-1. MOVEMENT OF FERMI LEVEL DUE TO LIGHT INDUCED DEFECTS.

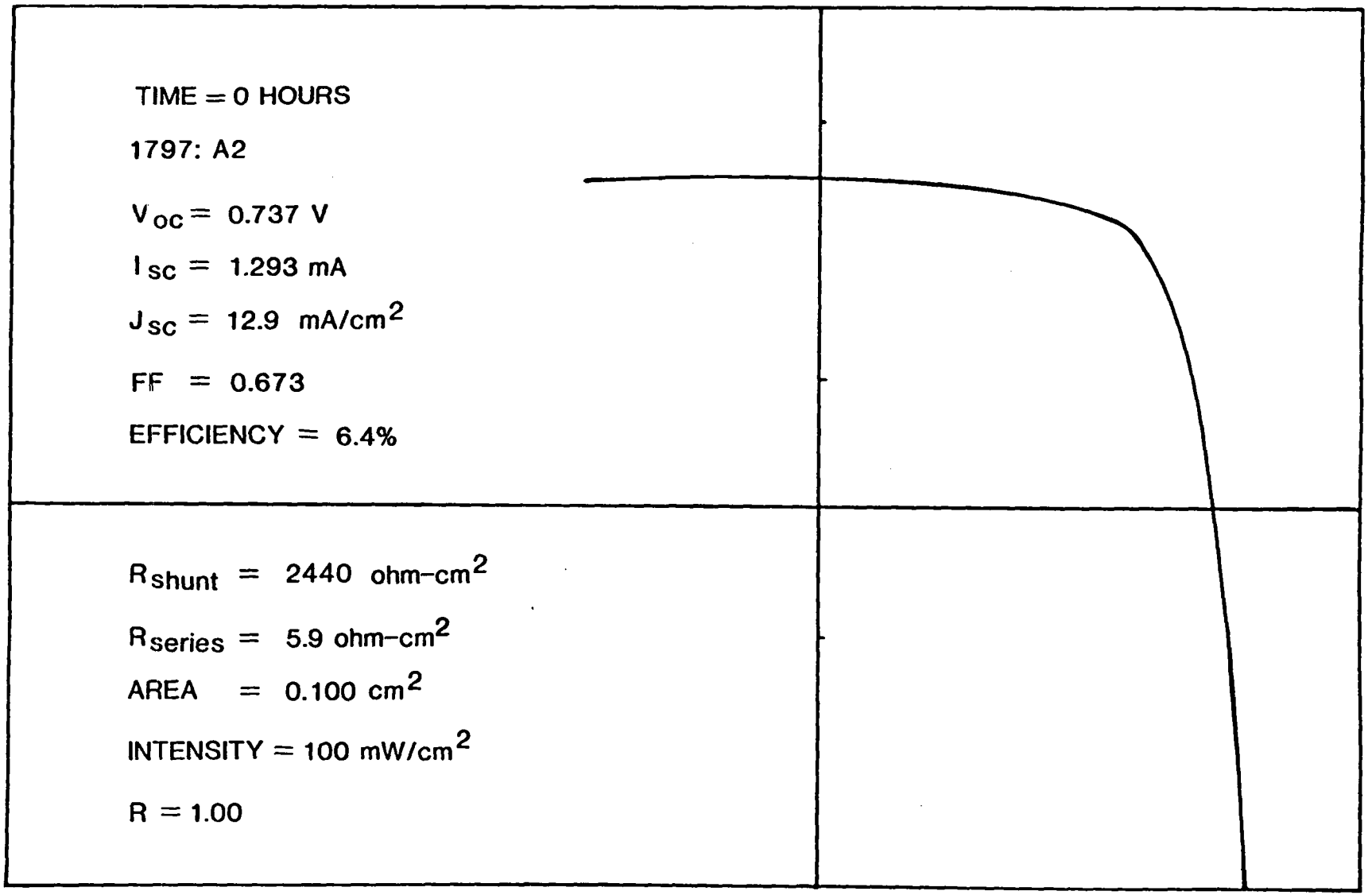

FIGURE B-2. SAMPLE #R1-1797.

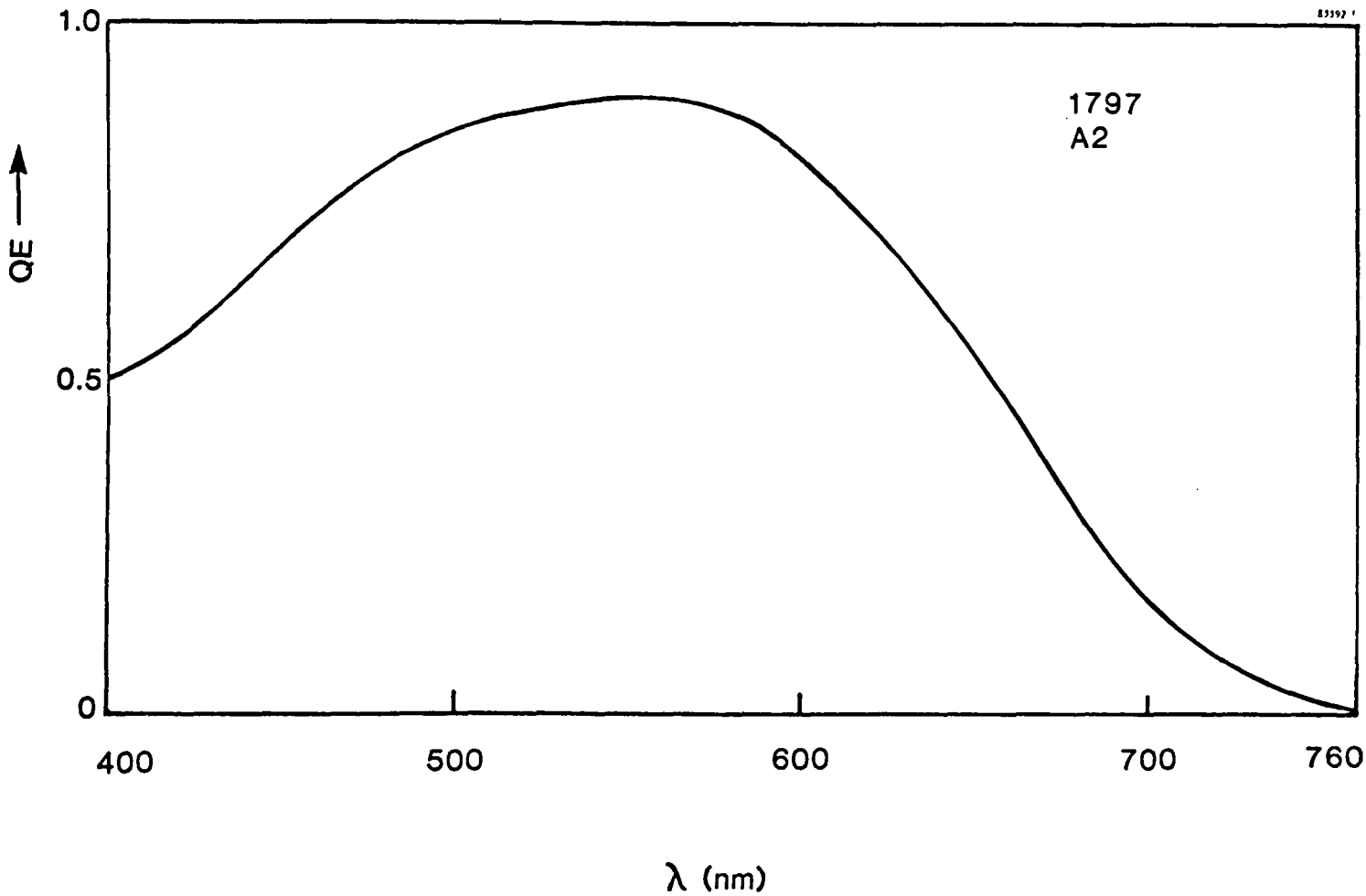

FIGURE B-3. QE FOR CELL OF FIGURE B-2.

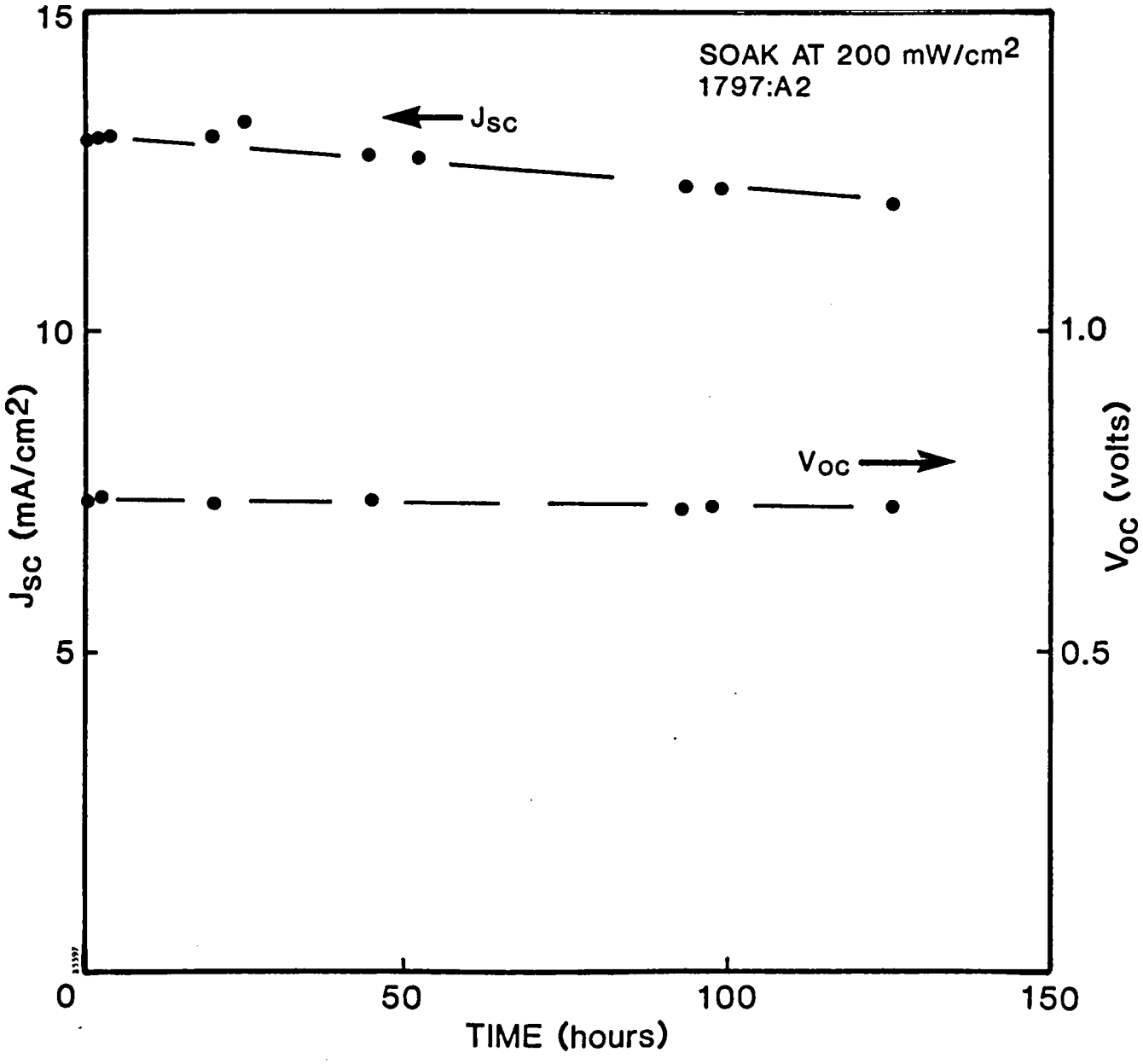

FIGURE B-4A. J_{sc} AND V_{oc} VS. TIME FOR SINGLE JUNCTION CELL.

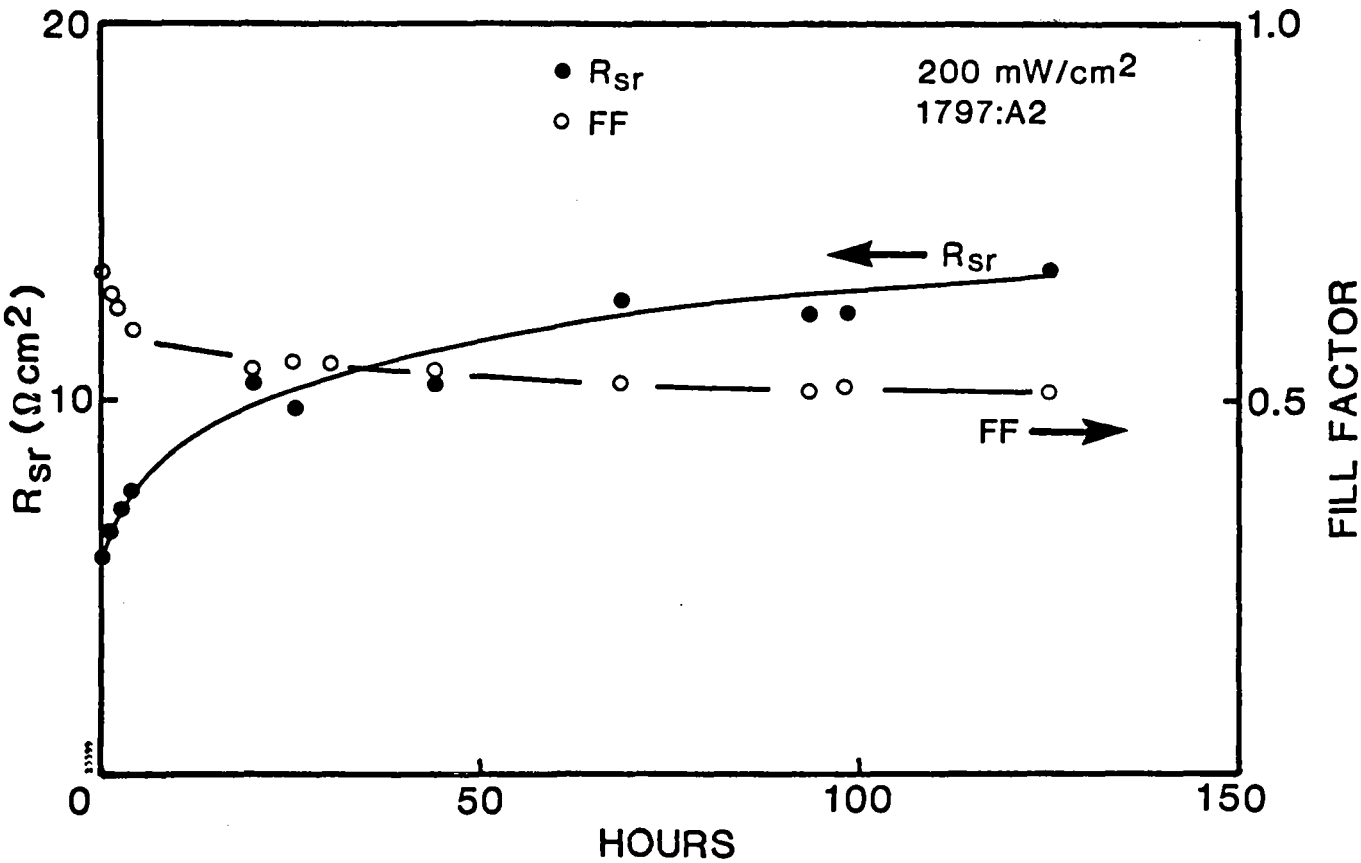

FIGURE B-4B. FILL FACTOR AND SERIES RESISTANCE VS. TIME. (Single Junction Cell.)

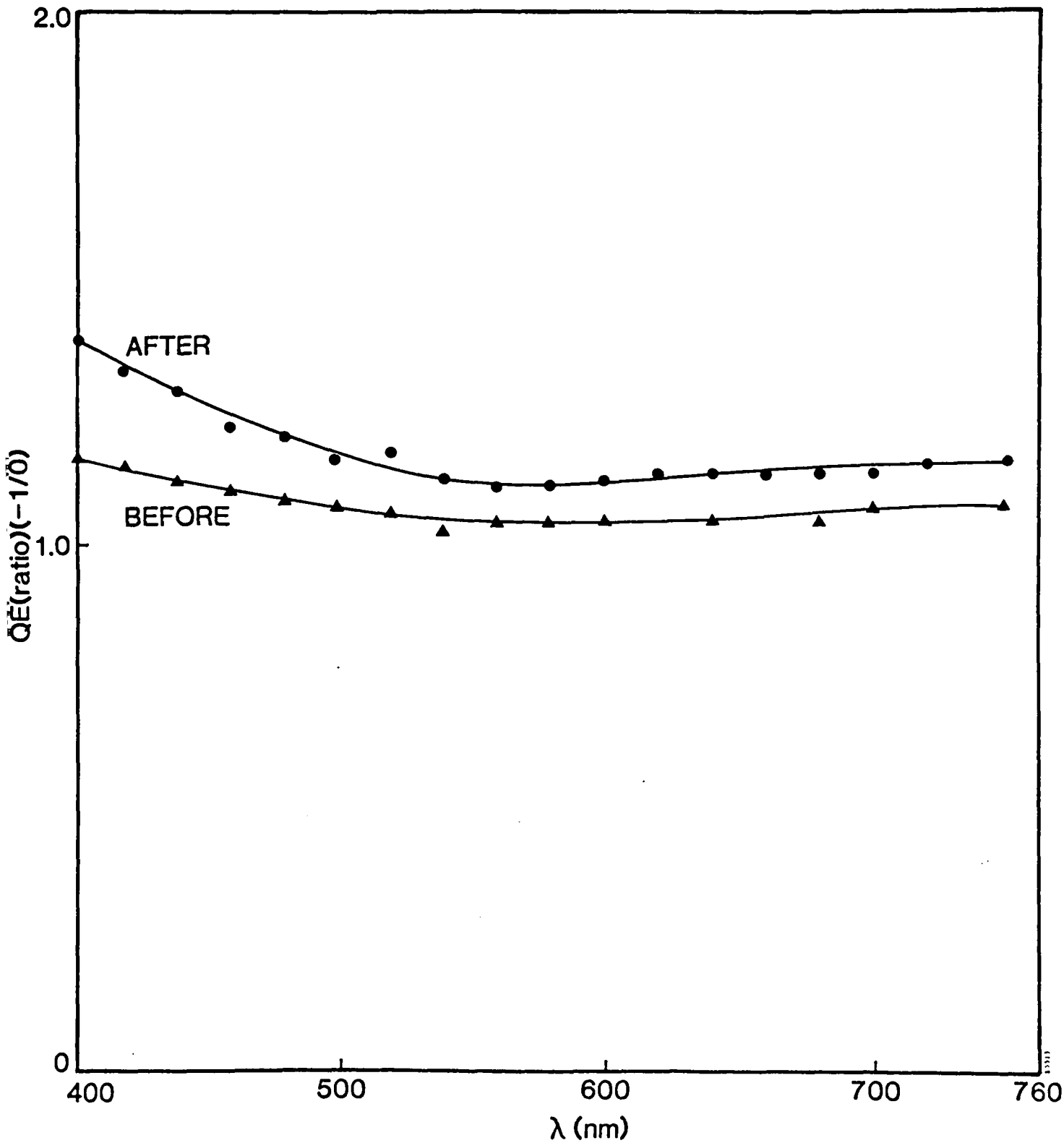

FIGURE B-5. QE RATIO BEFORE AND AFTER DEGRADATION.

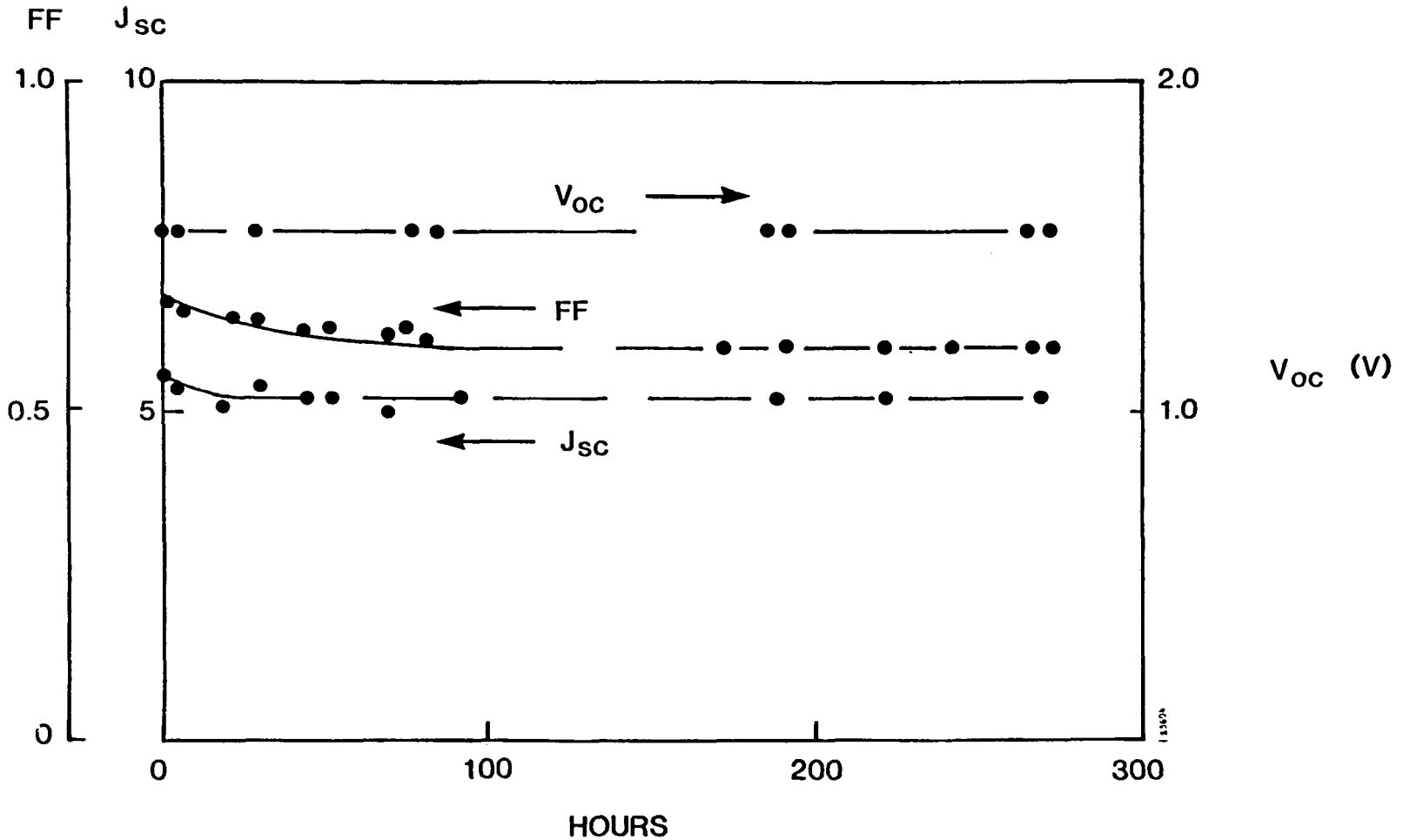

FIGURE B-6. BEHAVIOR OF DEVICE PARAMETERS OF TANDEM CELL 20135-C5 VS. TIME.

Document Control Page	1. SERI Report No. SERI/STR-211-3104	2. NTIS Accession No.	3. Recipient's Accession No.

4. Title and Subtitle
Research on High-Efficiency, Stacked, Multi-Junction, Amorphous Silicon Alloy Thin-Film Solar Cells, Semiannual Subcontract Report, 15 October 1985 - 30 April 1986

5. Publication Date
January 1987

6.

7. Author(s)
V. Dalal

8. Performing Organization Rept. No.

9. Performing Organization Name and Address
Spire Corporation
Bedford, MA 01730

10. Project/Task/Work Unit No.
3473.10

11. Contract (C) or Grant (G) No.
(C) ZB-4-03055-1
(G)

12. Sponsoring Organization Name and Address
Solar Energy Research Institute
A Division of Midwest Research Institute
1617 Cole Boulevard
Golden, Colorado 80401-3393

13. Type of Report & Period Covered
Technical Report

14.

15. Supplementary Notes
Technical Monitor: Werner Luft

16. Abstract (Limit: 200 words) This report describes work performed to investigate and develop high-efficiency, multijunction amorphous silicon alloy thin-film solar cells. Specifically, a-Si:H and a-(Si,Ge):H alloys have been deposited and characterized chemically, structurally, optically, and electronically. Also, a-Si:H/a-(Si,Ge):H high-efficiency tandem solar cells have been fabricated and analyzed. In this contract period, a plasma-isolated, two-chamber, hot-wall glow discharge reactor began operating. Good quality a-Si:H layers were grown. A chemical vapor deposition (CVD) pyrolytic reactor for depositing SnO_2:F layers on glass was also used. Single-junction a-Si:H cells up to 9.1% in efficiency were fabricated, as were multijunction a-Si:H/a-(Si,Ge):H cells up to 7.2% in efficiency.

17. Document Analysis
a. Descriptors Amorphous state ; silicon solar cells ; simiconductor materials ; chemical vapor deposition ; thin films

b. Identifiers/Open-Ended Terms

c. UC Categories
63

18. Availability Statement
National Technical Information Service
U.S. Department of Commerce
5285 Port Royal Road
Springfield, Virginia 22161

19. No. of Pages
68

20. Price
A04

Form No. 0069 (3-25-82)